
DECENTRALIZED NO-REGRET FREQUENCY-TIME SCHEDULING FOR FMCW RADAR INTERFERENCE AVOIDANCE

Yunian Pan,
 New York University,
 Brooklyn,
 NY, USA
 yp1170@nyu.edu

Jun Li
 NXP Semiconductors,
 San Jose,
 CA, USA
 jun.li_5@nxp.com

Lifan Xu
 The University of Alabama,
 Tuscaloosa,
 AL, USA
 lxu36@crimson.ua.edu

Shunqiao Sun
 The University of Alabama,
 Tuscaloosa,
 AL, USA
 shunqiao.sun@ua.edu

Quanyan Zhu
 New York University,
 Brooklyn,
 NY, USA
 qz494@nyu.edu

ABSTRACT

Automotive frequency modulated continuous wave (FMCW) radars are indispensable to modern advanced driver assistance system (ADAS) and autonomous-driving systems, but their increasing density has intensified the risk of mutual interference. Existing mitigation techniques, including reactive receiver-side suppression, proactive waveform design, and cooperative scheduling, often face limitations in scalability, reliance on side-channel communication, or degradation of range–Doppler resolution. Building on our earlier work on decentralized frequency-domain no-regret hopping, this paper introduces a unified time–frequency game-theoretic framework that enables radars to adapt across both spectral and temporal resources. We formulate the interference-avoidance problem as a repeated anti-coordination game, in which each radar autonomously updates a mixed strategy over frequency subbands and chirp-level time offsets using regret-minimization dynamics. We show that the proposed Time–Frequency No-Regret Hopping algorithm achieves vanishing external and swap regret, and that the induced empirical play converges to an ε -coarse correlated equilibrium or a correlated equilibrium. Theoretical analysis provides regret bounds in the joint domain, revealing how temporal adaptation implicitly regularizes frequency selection and enhances robustness against asynchronous interference. Numerical experiments with multi-radar scenarios demonstrate substantial improvements in SINR, collision rate, and range–Doppler quality compared with time-frequency random hopping and centralized Nash-based benchmarks.

Keywords automotive radar · game theory · frequency hopping · interference mitigation · interference avoidance

1 Introduction

High-resolution FMCW radars are central to ADAS and autonomous driving (AD), providing accurate range, velocity, and angle estimates under diverse environmental conditions [1–8]. FMCW radars enable hazard detection and autonomous decision-making, serving as a cornerstone of vehicle safety and autonomy, and are thus essential for both current and future vehicles.

1.1 Motivation

Modern automotive FMCW radars predominantly operate in the 76–81 GHz bands [9], with some systems, such as Forvia/Hella’s 3rd and 4th generations, also utilizing 24 GHz. While the 24 GHz ISM band offers limited

bandwidth (200–250 MHz depending on region), the 76–81 GHz band supports both long- and short-range sensing, making it central to ADAS. As radar adoption surges across automotive platforms, the risk of mutual interference has grown acute. Without effective interference mitigation, signal-to-interference-plus-noise ratio (SINR) deteriorates, compromising detection performance in safety-critical functions such as automatic emergency braking (AEB), vulnerable road user (VRU) protection, and adaptive cruise control (ACC). The importance of interference mitigation has been recognized across industry and regulatory bodies through initiatives such as the EU MOSARIM program, the NHTSA Radar Congestion Study [10], and Germany’s IMIKO-Radar project [11]. A broad line of research has since examined interference mitigation using orthogonal signaling, reactive receiver-side suppression, proactive waveform design, protocol-based scheduling, and more recently, vehicle-to-everything (V2X)-assisted coordination. Despite these developments, ensuring reliable radar operation under dense and heterogeneous deployments remains challenging. The limitations of centralized or communication-dependent approaches highlight the need for adaptive and fully decentralized interference-avoidance mechanisms.

1.2 Existing Interference Mitigation Approaches

A broad spectrum of interference mitigation strategies has been investigated to sustain the reliable operation of automotive radars under dense deployment [1,2]. These techniques can be broadly classified into three sub-categories.

1.2.1 Receiver-side suppression methods

focus on detecting and suppressing interference after reception. Common strategies include time-domain blanking or clipping [12], time-frequency thresholding [13–15], and adaptive filtering [16], which selectively remove contaminated portions of the received signal. More recent work leverages deep learning models such as score-based generative networks, recurrent neural networks, and attention mechanisms to identify and reconstruct interference-free signals [17–20]. Although these approaches can be effective in moderate interference conditions, their performance degrades when the number of interferers increases. In dense scenarios, interference often overlaps with the target echo in both the time domain and the time–frequency domain, making it fundamentally difficult to reliably separate and recover the original signal energy and thereby fully restore the Signal-to-noise Ratio (SNR). Moreover, some deep learning-based solutions may introduce additional latency or computational cost.

1.2.2 Transmitter-side (proactive) methods

aim to prevent interference before it occurs by diversifying radar waveforms. Classical techniques exploit orthogonality in time, frequency, or code domains, while more advanced designs employ nonlinear frequency hopping or multiband chirps to reduce collision probability while preserving range resolution [2, 4, 21, 22]. These approaches can improve the received SINR, but they also exhibit several limitations. Without coordination among radars, waveform diversification remains vulnerable to random overlap, especially in dense traffic where the available time–frequency space is limited. In addition, many waveform modifications introduce inherent trade-offs with sensing performance, including reduced range or velocity resolution, increased sidelobes, or degraded Doppler coherence. The resulting designs are often difficult to adapt in real time to rapidly changing interference conditions, and their effectiveness diminishes in heterogeneous environments where different radar platforms operate with different bandwidths, slopes, and timing configurations.

1.2.3 Cooperative and protocol-based methods

leverage communication between vehicles or radars to coordinate spectrum access. Examples include MAC-style scheduling [23], radar networking via LTE/5G, and radar–communication (RadCom) systems enabled by V2X links [24]. These methods can, in principle, guarantee interference-free operation, but they rely on robust side channels and synchronized participation, which may not be feasible in heterogeneous or adversarial settings.

1.3 No-Regret Hopping As a Hybrid Approach

To address the aforementioned issues, we introduced a game-theoretic framework for frequency scheduling in [25], where each radar is modeled as a strategic player that selects frequency-hopping schemes to optimize its own performance under mutual interference. In this formulation, the utility of each player is defined by its resulting SINR, and the goal is to learn adaptive hopping strategies that mitigate interference while preserving range resolution.

Within noncooperative game theory, two canonical solution concepts are often considered: 1) *Nash Equilibrium* (NE) [26], where no player has an incentive to unilaterally deviate from its chosen strategy. 2) *Coarse Correlated Equilibrium* (CCE) [27], a broader class of equilibria defined as joint distributions over strategies such that players

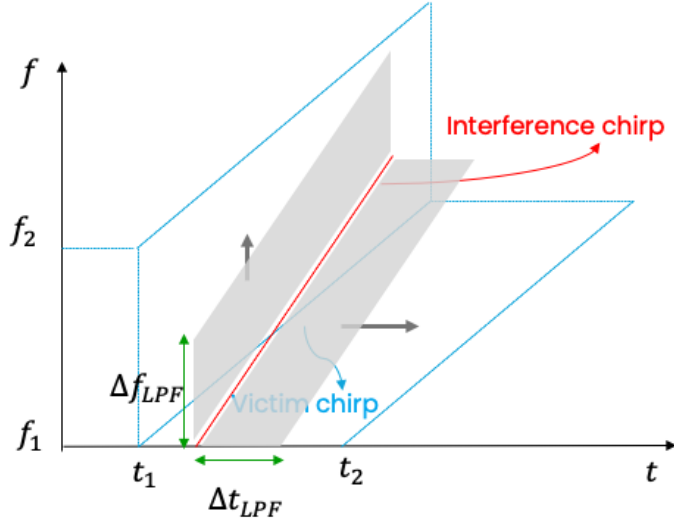


Figure 1: Illustration of interference mitigation through frequency and time shifting. When interference occurs, two potential adaptation directions are available (gray arrows).

cannot improve their expected utility by deviating from signaled recommendations. We demonstrated that due to the several drawbacks of NE in radar scenarios, namely equilibrium selection, price of anarchy, and computational infeasibility (PPAD-hard [28]). Learning a CCE turns out to be more computational feasible and economical [29–31]. Building on this insight, the proposed *No-Regret Hopping*, a decentralized algorithm that leverages regret minimization to approach a CCE, demonstrated several advantages: it requires no inter-radar communication, scales naturally to dense deployments, and empirically outperformed both the centralized *Nash Hopping* approach [32] and uniformly random hopping.

While these results established No-Regret Hopping as a robust frequency-domain solution, the framework in [25] remained restricted to probabilistic frequency allocation across chirps and therefore did not exploit the temporal dimension available between consecutive linear chirps. As illustrated in Fig. 1, limiting adaptation to frequency shifting alone overlooks the additional temporal resource, and independent subband sampling across chirps inevitably induces a trade-off between range resolution and interference avoidance. To overcome this limitation, the present work extends the no-regret learning framework into the *time-shifting domain*, enabling joint adaptation over both frequency and time. This extension enables a broader utilization of the allocable frequency-time resource.

1.4 Related Work and Contributions

Several prior studies [4] have explored time-domain techniques to mitigate radar interference in distributed environments. One common approach involves introducing chirp-level time shifts within a radar frame to reduce the likelihood of simultaneous transmissions from multiple devices. For example, some works propose random or pseudo-random time dithering of chirp start times to decorrelate overlapping signals and suppress coherent interference. These methods are particularly effective in uncoordinated settings where centralized scheduling is not feasible. In addition, time-division randomization has been shown to improve detection performance by spreading potential collisions across the slow-time dimension, thereby reducing persistent interference patterns. While these techniques can reduce interference probability, they are often used in isolation and may not fully exploit the benefits of combining time and frequency diversity. Our work builds on these insights by integrating slow-time chirp shifting with frequency hopping, aiming to achieve a more robust and scalable interference avoidance strategy in dense radar networks.

Time-shifting strategies. While most prior research on interference mitigation has focused on frequency-domain approaches, a growing body of work recognizes the importance of temporal alignment between chirps. Early reactive methods employed time-domain blanking or delay-based suppression to mitigate overlapping interference [12, 16], but these strategies do not proactively exploit the temporal degrees of freedom. More recent approaches have considered randomized pulse repetition intervals (PRIs) or asynchronous chirp scheduling [13, 24], which reduce collision

probability but lack formal guarantees and often degrade range–Doppler resolution. To the best of our knowledge, no existing work integrates time-domain shifting into a learning-theoretic framework with provable convergence guarantees.

Our contributions. This paper extends the previous *No-Regret Hopping* framework [25] in the frequency-domain into the time-shifting domain, thereby unifying frequency and temporal adaptation for FMCW radar interference avoidance. The main contributions are as follows:

- We reformulate the radar interference avoidance problem as a repeated game where radars adapt both their subband allocation and temporal chirp positioning, thus capturing the joint frequency–time trade-off.
- We develop a decentralized *Time–Frequency No-Regret Hopping* algorithm that guarantees vanishing external regret, leading to convergence toward an ε -Correlated/Coarse correlated equilibrium (CCE/CE), providing a theoretical analysis of regret bounds in the joint domain and demonstrating how implicit temporal regularization improves robustness against asynchronous interference.
- We validate the proposed framework through simulations that show significant improvements in SINR and target detection quality compared to purely randomized frequency-hopping-time-shifting strategy, and benchmark predetermined Nash equilibrium strategies.

Organization of the paper. The remainder of the paper is structured as follows. Section 2 introduces the radar signal model and formulates the interference avoidance game with joint frequency–time resources. Section 3 presents the proposed no-regret learning framework and provides theoretical analysis. Section 4 reports numerical simulations and performance evaluations. Finally, Section 5 concludes the paper and discusses future directions, including heterogeneous radar deployments and real-time implementation challenges.

2 Game Formulation and Signal Model

We consider a system comprising a set of automotive FMCW radars denoted by $\mathcal{I} = \{1, \dots, I\}$, each operating in real time to detect a single target object. Every radar transmits linear frequency modulated (LFM) chirps over a total bandwidth B^i centered at frequency f_c .

The radar operations span \mathcal{T} coherent processing intervals (CPIs), indexed by $\tau \in \{1, \dots, \mathcal{T}\}$, each CPI consists of duration T , within which a radar $i \in \mathcal{I}$ transmits K^i discrete chirps sequentially. For each chirp, the pulse repetition interval (PRI) for each radar i is given by $T_{\text{PRI}}^i = \frac{T}{K^i}$, which basically consists of an active period T_a^i and a dwell period T_d^i , such that

$$T_{\text{PRI}}^i = T_a^i + T_d^i, \quad \text{with} \quad T_d^i > 0.$$

During the active interval T_a^i , the radar emits a chirp that sweeps a subband of bandwidth B^i , yielding a chirp slope of $\alpha^i = \frac{B^i}{T_a^i}$.

We discretize the frequency and time resources as follows:

- The total bandwidth B_{tot} is partitioned into A_f (potentially overlapped) subbands $\{f_1, \dots, f_{A_f}\}$, where each subband has bandwidth B^i and is defined by a starting frequency $f_a = f_c + (a-1)\Delta f$, for $a \in \{1, \dots, A_f\}$ with Δf denoting the subband frequency offset (or hopping).
- The dwell duration T_d is illustrated in Figure 2. The dwell time is divided into A_t discrete time slots $\{t_1, \dots, t_{A_t}\}$, where each representing the starting time of the active period $t_b = (b-1)\Delta t$, for $b \in \{1, \dots, A_t\}$ with Δt denoting the chirp time domain shifting.

Hence, every chirp corresponds to a joint time–frequency action. The joint time–frequency action space is a Cartesian product $\mathcal{A} = \{f_1, \dots, f_{A_f}\} \times \{t_1, \dots, t_{A_t}\}$, so that radar i selects one subband f_a and one start time t_b per chirp.

2.1 Graphical Game Model

To proactively avoid interference, the radars strategically select frequency hopping and time shifting sequences $(f_1^i, t_1^i, \dots, f_{K^i}^i, t_{K^i}^i)$ across chirps within each CPI. We denote the composition of the channel selection and active period selection strategies of radar i by $\sigma^i(\cdot) : \{1, \dots, K^i\} \rightarrow \mathcal{A}$; for example, $\sigma^i(k) = (f, t)$ indicates that radar i selects subband $[f, f + B]$ at chirp k , sending one LFM pulse between $[t, t + T_a]$. Let Σ^i denote the strategy set of radars i . Note that Σ^i does not necessarily exhaust all possible mappings; for instance, it may be defined as a set of periodic mappings with an offset n , that is, $\Sigma^i := \{\sigma \mid \sigma_1(k) = k + n \bmod K^i, n \in \mathbb{N}\}$. Note that in general, the design of the strategy sets is not restricted to such configurations.

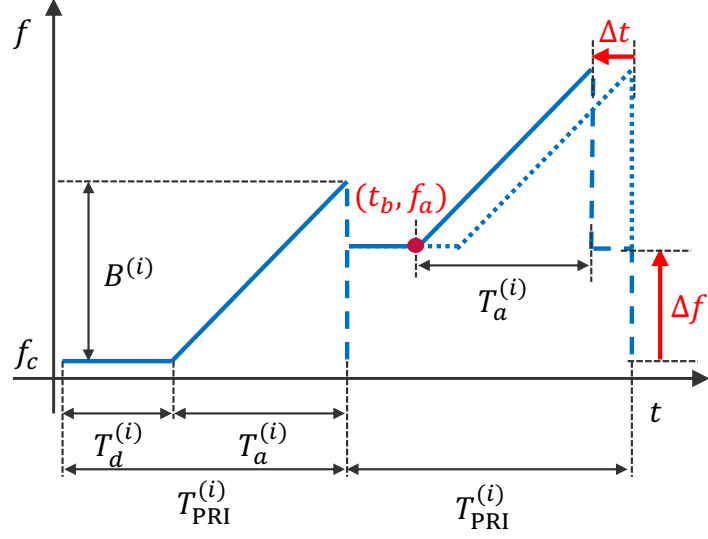


Figure 2: Joint time–frequency scheduling illustration. Each chirp selects a subband start f_a and a time offset t_b within the dwell segment $T_d^{(i)}$. The subband frequency hopping and time shifting width are Δf and Δt , forming the joint action (t_b, f_a) .

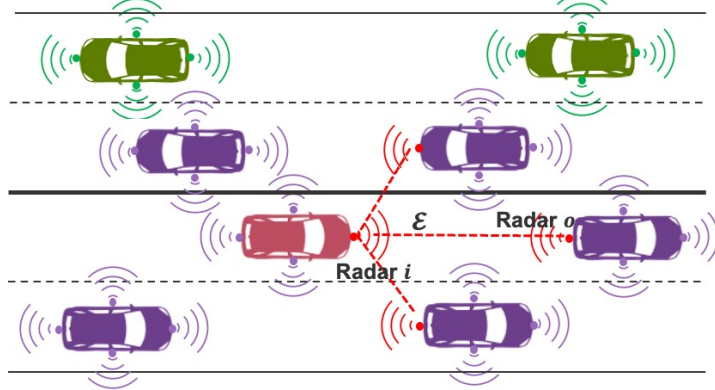


Figure 3: Typical automotive radar interference scenario. The red vehicle’s front radar receives interference from three radars on nearby purple vehicles, i.e., two front-facing and one rear-facing. Mutual interference links among these distributed radars form a graphical game representation.

Then, the typical radar-to-radar interference scenario as shown in Fig. 3 can be modeled as a \mathcal{T} -stage repeated graphical game $\Gamma = \{\mathcal{I}, \{\Sigma^i\}_{i \in \mathcal{I}}, \mathcal{G}, \{U^i\}_{i \in \mathcal{I}}\}$, where the stages \mathcal{T} are CPIs; the radars, acting as players in \mathcal{I} , share a common strategy set Σ . The interference relationships among a set of radars are modeled by a weighted, directed graph $\mathcal{G} = (\mathcal{I}, \mathcal{E}, \Delta)$, where each node $i \in \mathcal{I}$ corresponds to radar i , and each directed edge $(i \rightarrow o) \in \mathcal{E}$ indicates that radar i can interfere with radar o . In addition, each directed edge $(i \rightarrow o) \in \mathcal{E}$ carries a delay Δ_{io} (seconds), the arrival-time offset of radar i ’s waveform as measured in radar o ’s local clock. We assume \mathcal{G} is CPI-invariant for simplicity. Therefore, \mathcal{G} fully specifies who interferes with whom and when. In this work, we assume \mathcal{G} is stage independent for simplicity. The (also stage-independent) utility functions $U^i : \prod_{i \in \mathcal{I}} \Sigma^i \rightarrow \mathbb{R}$ endows this game with the anti-coordination property, where the pulse transmission strategies σ^i employed by players are from potentially different strategy sets Σ^i , but whenever two or more radar’s transmission strategies agree, say, $\sigma^i(k) \approx \sigma^o(k)$ at chirp k for some radars i and o , the utilities of radar i and o decrease because (f_k^i, t_k^i) being close to (f_k^o, t_k^o) will defect the detection ability of both radar i and o if there is interference between these two, i.e., $(i, o) \in \mathcal{E}$ and t_k^i and $t_k^o + \Delta_{io}$ are close enough. In this paper, we give the following definition for players’ utility functions, for each stage $\tau = 1, \dots, \mathcal{T}$,

$$U^i(\sigma_\tau^i, \sigma_{\tau}^{-i}) = u(\text{SINR}_\tau^i), \quad (1)$$

where SINR_τ^i represents the average obtained SINR of CPI $\tau \in \{1, \dots, \mathcal{T}\}$, at radar i 's receiver, determined by the joint strategies $\sigma_\tau^i, \sigma_{\tau}^{-i}$ for CPI τ ; $u(\cdot)$ ¹ is a strictly increasing differentiable function that maps the SINR to a scalar in $(0, 1)$. The scalar \bar{U}_τ^i is appended to the utility buffer \mathcal{U} and fed to one of the regret-minimization subroutines. In the absence of interference, the SINR reduces to the signal-to-noise ratio (SNR). In what follows, we formally present the signal modeling and processing, interference modeling and filtering, and output SINR estimation.

2.2 Signal Model and Match Filtering

Let radar $i \in \mathcal{I}$ adopt a transmission strategy σ^i , consisting of a sequence of starting frequencies $(f_k^i)_{k=1}^{K^i}$ and a sequence of start times $(t_k^i)_{k=1}^{K^i}$ for each of the K^i transmitted chirps. Consider $\mathcal{L} := \{1, \dots, L\}$ targets within its field of view, with range vector $(r_\ell^i)_{\ell=1}^L$ and velocity vector $(\dot{r}_\ell^i)_{\ell=1}^L$. Approaching targets satisfy $r_\ell^i < 0$.

The transmitted LFM signal at the k -th chirp is modeled as:

$$s_{\text{tx}}^i[t, k] = \begin{cases} e^{j2\pi(f_k^i(t-t_k^i) + \frac{1}{2}\alpha^i(t-t_k^i)^2)}, & t_k^i \leq t < t_k^i + T_a^i, \\ 0, & \text{otherwise} \end{cases}$$

and the received echo from the ℓ^{th} target is then given by:

$$s_{\text{rx}}^i[t, k] = \begin{cases} a_\ell^i s_{\text{tx}}^i[t - \tau_{k,\ell}^i, k], & t_k^i + \tau_{k,\ell}^i \leq t < t_k^i + \tau_{k,\ell}^i + T_a^i, \\ 0, & \text{otherwise,} \end{cases}$$

where a_ℓ^i is the complex target coefficient and $\tau_{k,\ell}^i$ is the round trip delay at chirp k , given by $\tau_{k,\ell}^i = \frac{2}{c} [r_\ell^i + \dot{r}_\ell^i(kT_{\text{PRI}}^i - T_{\text{PRI}}^i + t_k^i - t_1^i)]$, with c denoting the speed of light.

The echo signal, mixed with the transmitted signal, yields the system output:

$$\begin{aligned} y^i[t, k] &= \sum_{\ell=1}^L a_\ell^i s_{\text{tx}}^i[t, k] s_{\text{rx}}^{i*}[t, k] \\ &\approx \sum_{\ell=1}^L \tilde{a}_\ell^i e^{j2\pi(f_k^i \tau_{k,\ell}^i + \alpha^i \tau_{k,\ell}^i t)}, \end{aligned}$$

where constant terms are consolidated in the complex target coefficient \tilde{a}_ℓ^i and the coarse range migration across chirps [22] is negligible due to small chirps with short bandwidth B^i .

To decouple coarse and fine range components, the target range is decomposed as $r_\ell^i + \dot{r}_\ell^i(kT_{\text{PRI}}^i - T_{\text{PRI}}^i + t_k^i - t_1^i) = \bar{r}_\ell^i + [\epsilon_\ell^i + \dot{\epsilon}_\ell^i(kT_{\text{PRI}}^i - T_{\text{PRI}}^i + t_k^i - t_1^i)]$, where \bar{r}_ℓ^i denotes the coarse range center of ℓ^{th} target with bin width $\frac{c}{2B^i}$, and $\epsilon_\ell^i \in [-\frac{c}{4B^i}, \frac{c}{4B^i}]$ is the fine offset.

Then the received echo becomes:

$$\begin{aligned} y^i[t, k] &= \sum_{\ell=1}^L \tilde{a}_\ell^i e^{j2\pi(f_k^i \tau_{k,\ell}^i + \alpha^i \tau_{k,\ell}^i t)} \\ &= \sum_{\ell=1}^L \tilde{a}_\ell^i e^{j2\pi[f_R t + f_D(kT_{\text{PRI}}^i - T_{\text{PRI}}^i + \Delta t_k^i) + \Delta f_k^i \tau_{k,\ell}^i]} \end{aligned}$$

where the hopping frequency offset is defined as $\Delta f_k^i = f_k^i - f_c$ and the time shift as $\Delta t_k^i = t_k^i - t_1^i$. The coarse range frequency is $f_R := \alpha^i \frac{2r_\ell^i}{c}$, and the Doppler frequency is $f_D := f_c \frac{2\dot{r}_\ell^i}{c}$. Without frequency hopping and time shifting (i.e., $\Delta f_k^i = 0$ and $\Delta t_k^i = 0$), the signal reduces to the standard form. Otherwise, the term $\Delta f_k^i \tau_{k,\ell}^i$ enables finer range resolution [25], while the term Δt_k^i introduces a nonuniform pulse repetition frequency (PRF). Note that this nonuniform PRF will yield high sidelobes in the Doppler spectrum and can be solved by advanced algorithms such as compressed sensing (CS) or joint range-Doppler processing [33] which is another important topic and is

¹In practice we use a saturating map $g(s) = \frac{s^\beta}{s^\beta + S_0^\beta}$ on linear SINR, with $\beta \in (0, \infty)$ and S_0 the “half-good” SINR; this facilitates algorithmic stability.

out of the scope of this paper. Since Doppler resolution is primarily determined by the coherent processing interval (CPI), the time shift Δt_k^i , constrained within T_{PRI}^i , does not change the resolution but increases the likelihood of interference avoidance by randomizing chirp starting timings. Note that such nonuniform transmission along slow time significantly reduces the probability that a victim radar experiences persistent interference compared with uniform transmission. In practical deployments, when two radars share similar T_{PRI} values, interference between their first overlapping chirps often persists across subsequent chirps under uniform transmission.

Let $\mathbf{Y}^i \in \mathbb{C}^{N_t^i \times K^i}$ be the down-sampled and low-pass filtered ADC matrix for radar i with columns indexed by chirp k and rows by fast-time samples n . We process \mathbf{Y}^i in three steps, i.e., fast-time processing, frequency hopping and time shifting compensation, nonuniform slow-time processing, yielding coarse range, fine range, and Doppler (velocity) estimates.

1) Coarse-range processing Apply a fast-time coherent integration processing per chirp:

$$\mathbf{Y}_{\text{cr}}^i = \mathbf{R}^i \mathbf{Y}^i, \quad R_{n,m}^i = e^{-j \frac{2\pi}{N_t^i} nm}, \quad n, m = 0, \dots, N_t^i - 1, \quad (2)$$

which maps fast time to coarse range bins $r_m = \bar{r}_\ell^i$.

2) Joint frequency-time compensation For each coarse bin m , chirp k , and a candidate fine-range offset $\epsilon_p \in [-\frac{c}{4B^i}, \frac{c}{4B^i}]$, construct

$$\begin{aligned} Y_{cp}^i[m, k, p] \\ = Y_{cr}^i[m, k] e^{j2\pi \left(\Delta f_k^i \left(\frac{2r_m}{c} + \frac{2\epsilon_p}{c} + \frac{2v_q(kT_{\text{PRI}}^i - T_{\text{PRI}}^i + \Delta t_k^i)}{c} \right) \right)}, \end{aligned} \quad (3)$$

where Δf_k^i and t_k^i are known by the radar i receiver, v_q is a velocity-grid value used when forming a joint (ϵ_p, v_q) hypothesis. The exponential term aligns inter-chirp phases introduced by frequency hopping and time-shifting so that fine-range information becomes coherent across k .

3) Nonuniform slow-time processing For each p and q -grid used in (3), apply the slow-time nonuniform matching along chirp index k :

$$\mathbf{Y}_{\text{out}}^i[:, q, p] = \mathbf{Y}_{\text{cp}}[:, :, p] \mathbf{D}^i(:, q) \quad (4)$$

and

$$D_{k,q}^i = e^{-j \frac{2\pi(kT_{\text{PRI}}^i - T_{\text{PRI}}^i + \Delta t_k^i)}{K^i T_{\text{PRI}}^i} q}, \quad (5)$$

which forms a Range–Doppler (and fine-range) cube $Y_{\text{out}}^i[m, q, p]$. We then select the global peak $(m^*, q^*, p^*) = \arg \max_{m,q,p} |Y_{\text{out}}^i[m, q, p]|$, and read off the estimates $\hat{r} = r_{m^*} + \epsilon_{p^*}$, $\hat{v} \leftrightarrow q^*$.

2.3 Interference Model and SINR Estimation

At radar i ’s receiver, the target echoes may be corrupted by interference from other interfering radars $o \in \text{neighbor}(\{i\})$, each transmitting at its own f_k^o .

$$s_{tx}^o[t, k] = \begin{cases} e^{j2\pi(f_k^o(t - \Delta_{io} - t_k^o) + \frac{1}{2}\alpha^o(t - \Delta_{io} - t_k^o)^2)}, \\ \quad t_k^i \leq t < t_k^i + T_a^i, \\ 0, \quad \text{otherwise} \end{cases}$$

Interference arises when the starting frequencies overlap, i.e., $f_k^o = f_k^i$, and $\Delta_{io} + t_k^o$ is close to t_k^i . After demodulation and dechirping, the interference from radar o is:

$$y^o[t, k] \approx \tilde{a}^o e^{j\pi(\alpha^i - \alpha^o)t^2},$$

where α^o is the slope of the interfering chirp. This signal behaves as a chirp with slope $\alpha^i - \alpha^o$ and depends on time-frequency offsets between radar i and o [12].

The overall received signal at radar i ’s is then:

$$\hat{\mathbf{y}}^i = \mathbf{y}^i + \sum_{o \in \mathbf{N}_i} \mathbf{y}^o + \mathbf{e}^i, \quad (6)$$

where $\mathbf{y}^i = \{y^i[t, k]\}$ is the desired (analogue) signal, (we have used \mathbf{Y}^i to denote the doown-sampled and low-pass filtered digital signal) $\sum_{o \in \mathbf{N}_i} \mathbf{y}^o$ is the interference signal aggregation from all the neighbors of radar i in \mathcal{G} , i.e., $o \in \mathbf{N}_i \Rightarrow (o \rightarrow i) \in \mathcal{E}$, and \mathbf{e}^i is the white noise. Note that here we omit the CPI index.

Let $P(\cdot)$ denote average signal power. The theoretical SINR for radar i at CPI τ is expressed as:

$$\text{SINR}_\tau^i = \frac{P(\mathbf{y}_\tau^i)}{P(\sum_{o \in \mathbf{N}_i} \mathbf{y}_\tau^o) + P(\mathbf{e}_\tau^i)} \quad (7)$$

We assume that each radar estimates per-action SINR using its own receiver (RX) pipeline at the end of every CPI, without an extra side-channel required. The actual computation requires interference detection (e.g., thresholding [12]), and separating the signal into a clean part $\hat{\mathbf{y}}_\tau^i$ and an interference part $\hat{\mathbf{y}}_\tau^o$. In practice, due to limited observability, the ground truth SINR values are infeasible. We defer the estimation method to Section 3.

3 Solution Concepts and Algorithm Design

3.1 Frequency-time Scheduling with Mixed Strategy

We equip each radar i with an adaptable mixed strategy p_τ^i throughout CPI $\tau = 1, \dots, \mathcal{T}$. A mixed strategy is a probability distribution over the (deterministic) strategy class Σ^i , i.e., $p_\tau^i \in \Delta(\Sigma^i) := \{p : \Sigma^i \rightarrow [0, 1] \mid \sum_{\sigma \in \Sigma^i} p(\sigma) = 1\}$. Before the start of CPI τ , radar i samples a transmission strategy $\sigma_\tau^i \sim p_\tau^i(\cdot)$ and then executes it deterministically across the K^i chirps, which induces a per-chirp sequence of time–frequency pairs $\{(f_k^i, t_k^i)\}_{k=1}^{K^i}$. In essence, mixed strategies generate diverse chirp sequences that sustain target detection while mitigating mutual interference.

Let $U_i(\sigma_\tau^i, \sigma_\tau^{-i})$ be radar i ’s CPI utility (1), computed from the RX pipeline as $u(10 \log_{10}(\text{SINR}_\tau^i))$. The *expected* CPI utility under independent mixed strategies p_τ^i and p_τ^{-i} is

$$\bar{U}_i(p_\tau^i, p_\tau^{-i}) = \mathbb{E}_{\sigma_\tau^i \sim p_\tau^i, \sigma_\tau^{-i} \sim p_\tau^{-i}} [U_i(\sigma_\tau^i, \sigma_\tau^{-i})]. \quad (8)$$

Each radar updates p_τ^i online, from local measurements only, to maximize its long-term utility. In classical noncooperative game theory, when players act independently according to their own mixed strategies, the system may reveal a *Nash equilibrium* (NE) [26].

Definition 1. For the \mathcal{T} -stage repeated game $\Gamma = \{\mathcal{I}, \Sigma, \mathcal{G}, \{U_i\}_{i \in \mathcal{I}}\}$, a joint strategy profile (p^1, \dots, p^I) constitutes a Nash equilibrium if no radar can unilaterally improve its expected utility, i.e.,

$$\bar{U}_i(p^i, p^{-i}) \geq \bar{U}_i(p^i, p^{-i}), \quad \forall p^i \in \Delta(\Sigma^i), \forall i \in \mathcal{I}. \quad (9)$$

Intuitively, under an NE each radar’s mixed strategy is an optimal response to the others’ strategies, and no player has incentive to deviate. However, in radar interference scenarios, purely independent mixed strategies are often insufficient to ensure interference-free operation due to a variety of reasons discussed in [25]. Even when a Nash equilibrium exists, it often suffers from several fundamental limitations: (i) an equilibrium selection problem, since multiple equilibria may coexist and independent learners can converge to inconsistent or colliding strategies; (ii) suboptimality, as individual optimality does not imply maximal collective performance, often resulting in degraded overall SINR and inefficient spectrum utilization; and (iii) computational intractability, as finding a Nash equilibrium is known to be a PPAD-complete problem [28].

3.2 Correlated Equilibria and Coarse Correlated Equilibria

To overcome these limitations, a richer notion of equilibrium allows players’ actions to be statistically *correlated* through shared experience or endogenous signals. In this setting, the joint distribution over strategies, denoted by $\pi \in \Delta(\prod_{i \in \mathcal{I}} \Sigma^i)$, need not decompose into a product of marginals. *Correlated strategies* capture coordination patterns that emerge through repeated interaction and learning, enabling the system to approach equilibria with higher collective utility. Rather than assuming independent sampling of strategies, we let each radar draw its strategy recommendation from π and can decide whether to follow it or deviate. This framework generalizes the aforementioned setting, which corresponds to the special case in which π factorizes as the product of independent marginals.

Definition 2. For the \mathcal{T} -stage repeated game $\Gamma = \{\mathcal{I}, \{\Sigma^i\}_{i \in \mathcal{I}}, \mathcal{G}, \{U_i\}_{i \in \mathcal{I}}\}$, let $\pi \in \Delta(\prod_{i \in \mathcal{I}} \Sigma^i)$ denote a joint probability distribution over the players’ strategy profiles. Then:

a) π is a *Correlated Equilibrium* (CE) if, for every radar $i \in \mathcal{I}$ and for all $\sigma^i, \sigma^{i'} \in \Sigma^i$,

$$\mathbb{E}_{\sigma^{-i} \sim \pi(\cdot | \sigma^i)} [U_i(\sigma^i, \sigma^{-i})] \geq \mathbb{E}_{\sigma^{-i} \sim \pi(\cdot | \sigma^i)} [U_i(\sigma^{i'}, \sigma^{-i})]. \quad (10)$$

That is, once a joint strategy σ is drawn from π and radar i learns its own recommendation σ^i , it cannot improve its expected utility by deviating to another strategy $\sigma^{i'}$.

b) π is a *Coarse Correlated Equilibrium* (CCE) if, for every radar $i \in \mathcal{I}$ and for all $\sigma^{i'} \in \Sigma^i$,

$$\mathbb{E}_{\sigma \sim \pi} [U_i(\sigma^i, \sigma^{-i})] \geq \mathbb{E}_{\sigma \sim \pi} [U_i(\sigma^{i'}, \sigma^{-i})]. \quad (11)$$

In this case, radar i decides whether to deviate before seeing its recommended strategy, and such deviation cannot increase its expected utility.

A CCE is a relaxation of CE in which deviation decisions are made *before* observing any recommendation. Hence, every CE is a CCE, but the converse does not always hold; the set of CCE is larger and typically easier to approach in practice.

In general, computing CE or CCE directly requires solving systems of linear inequalities of the form (10)–(11), whose size grows exponentially with the number of radars and the complexity of their strategy spaces [27]. However, centralized planning is infeasible in the radar-to-radar interference setting as it requires information exchange infrastructure. Therefore, we resort to *no-regret learning* to obtain these equilibria, where each radar independently updates its mixed strategy based on local utility feedback.

Definition 3. The *external regret* for radar i after \mathcal{T} CPIs is defined, given a sequence of fixed strategy profiles $\{\sigma_\tau^i, \sigma_\tau^{-i}\}_{\tau=1}^{\mathcal{T}}$, as:

$$\mathcal{R}_{\text{ext}}^i(\mathcal{T}) = \max_{\sigma^i \in \Sigma^i} \sum_{\tau=1}^{\mathcal{T}} [U_i(\sigma^i, \sigma_\tau^{-i}) - U_i(\sigma_\tau^i, \sigma_\tau^{-i})]. \quad (12)$$

External regret measures how much worse a radar performs compared to the best fixed strategy in hindsight. A learning process achieves *no external regret* if $\mathcal{R}_{\text{ext}}^i(\mathcal{T})/\mathcal{T} \rightarrow 0$ as $\mathcal{T} \rightarrow \infty$, meaning radar i performs asymptotically as well as the best fixed strategy in hindsight.

The notion of *internal regret*, also known as *swap regret*, refines and generalizes this benchmark by considering deviations from each played strategy to alternative ones according to a deterministic *swap mapping*.

Definition 4. Let $\phi^i : \Sigma^i \rightarrow \Sigma^i$ be a mapping that prescribes, for every strategy $\sigma^i \in \Sigma^i$, an alternative strategy $\phi^i(\sigma^i)$ to which radar i would have switched whenever σ^i was selected. The cumulative internal (swap) regret of radar i after \mathcal{T} CPIs is defined, given a sequence of fixed strategy profiles $\{\sigma_\tau^i, \sigma_\tau^{-i}\}_{\tau=1}^{\mathcal{T}}$, as

$$\mathcal{R}_{\text{int}}^i(\mathcal{T}) = \max_{\phi^i : \Sigma^i \rightarrow \Sigma^i} \sum_{\tau=1}^{\mathcal{T}} [U_i(\phi^i(\sigma_\tau^i), \sigma_\tau^{-i}) - U_i(\sigma_\tau^i, \sigma_\tau^{-i})]. \quad (13)$$

A learning process is said to have *no internal regret* if $\mathcal{R}_{\text{int}}^i(\mathcal{T})/\mathcal{T} \rightarrow 0$ as $\mathcal{T} \rightarrow \infty$. Intuitively, this means that no systematic replacement rule—swapping each previously played strategy σ^i with another $\phi^i(\sigma^i)$ —would have yielded higher average utility.

3.3 No-Regret Learning

A key result from learning in games [27, 34, 35] establishes a fundamental bridge between regret minimization and equilibrium concepts. When players iteratively update their mixed strategies to minimize regret, the empirical distribution of play converges to an equilibrium notion consistent with the form of regret being minimized. Specifically, minimizing *external regret* leads to convergence to a *coarse correlated equilibrium* (CCE), while minimizing the stronger *internal (swap) regret* yields convergence to a *correlated equilibrium* (CE).

Let the empirical joint distribution of strategies after \mathcal{T} CPIs be

$$\bar{\pi}(\sigma) := \frac{1}{\mathcal{T}} \sum_{\tau=1}^{\mathcal{T}} \mathbb{1}\{\sigma_\tau = \sigma\}, \quad \sigma = (\sigma^1, \dots, \sigma^I) \in \prod_{i \in \mathcal{I}} \Sigma^i, \quad (14)$$

where σ_τ denotes the joint strategy profile played at CPI τ .

Lemma 1. Suppose each radar $i \in \mathcal{I}$ achieves average internal (swap) regret at most ε , i.e.,

$$\frac{1}{\mathcal{T}} \max_{\phi^i: \Sigma^i \rightarrow \Sigma^i} \sum_{\tau=1}^{\mathcal{T}} \left[U_i(\phi^i(\sigma_\tau^i), \sigma_\tau^{-i}) - U_i(\sigma_\tau^i, \sigma_\tau^{-i}) \right] \leq \varepsilon, \quad (15)$$

where ϕ^i is a swap mapping prescribing, for each strategy σ^i , an alternative $\phi^i(\sigma^i)$. Then, the empirical distribution $\bar{\pi}$ is an ε -correlated equilibrium.

Proof. Fix $i \in \mathcal{I}$ and two strategies $\hat{\sigma}^i, \tilde{\sigma}^i \in \Sigma^i$. Define a pairwise swap mapping $\phi_{\hat{\sigma}^i \rightarrow \tilde{\sigma}^i}^i(\sigma^i) = \tilde{\sigma}^i$ if $\sigma^i = \hat{\sigma}^i$ and σ^i otherwise. Substituting $\phi_{\hat{\sigma}^i \rightarrow \tilde{\sigma}^i}^i$ into (15) yields

$$\frac{1}{\mathcal{T}} \sum_{\tau=1}^{\mathcal{T}} \mathbb{1}\{\sigma_\tau^i = \hat{\sigma}^i\} \left[U_i(\hat{\sigma}^i, \sigma_\tau^{-i}) - U_i(\tilde{\sigma}^i, \sigma_\tau^{-i}) \right] \geq -\varepsilon.$$

Recognizing the left-hand side as an expectation under $\bar{\pi}$ gives (16).

$$\mathbb{E}_{\sigma \sim \bar{\pi}} \left[\mathbb{1}\{\sigma^i = \sigma\} (U_i(\sigma^i, \sigma^{-i}) - U_i(\sigma^{i'}, \sigma^{-i})) \right] \geq -\varepsilon, \quad (16)$$

Dividing by $\bar{\pi}(\sigma^i)$ (if nonzero) yields the conditional form (17).

$$\mathbb{E}_{\sigma \sim \bar{\pi}(\cdot | \sigma^i)} [U_i(\sigma^i, \sigma^{-i})] \geq \mathbb{E}_{\sigma \sim \bar{\pi}(\cdot | \sigma^i)} [U_i(\sigma^{i'}, \sigma^{-i})] - \frac{\varepsilon}{\bar{\pi}(\sigma^i)}. \quad (17)$$

Since this holds for all i, σ^i , and $\sigma^{i'}$, $\bar{\pi}$ satisfies the ε -CE inequalities. \square

Corollary 1. External regret is a special case of internal (swap) regret, obtained by restricting the swap mapping to a constant function,

$$\phi^i(\sigma^i) \equiv \sigma^{i'}, \quad \forall \sigma^i \in \Sigma^i.$$

Hence, if each radar achieves vanishing external regret, the empirical distribution $\bar{\pi}$ satisfies the relaxed inequalities of an ε -coarse correlated equilibrium (CCE):

$$\mathbb{E}_{\sigma \sim \bar{\pi}} [U_i(\sigma^i, \sigma^{-i})] \geq \mathbb{E}_{\sigma \sim \bar{\pi}} [U_i(\sigma^{i'}, \sigma^{-i})] - \varepsilon, \quad \forall i \in \mathcal{I}.$$

Consequently, minimizing swap regret implies minimizing external regret and guarantees convergence to both CE and CCE.

In the context of radar interference avoidance, these results imply that when each radar locally minimizes its own regret, the empirical average of collective radar behavior asymptotically converges to a CE—a decentralized operating regime that balances interference avoidance with detection performance without side-channel coordination.

3.4 Algorithmic Design under Semi-Bandit Feedback

Algorithm 1 No-Regret Hopping for radar $i \in \mathcal{I}$

Require: initial strategy $p_1^i = \text{Unif}(\Sigma^i)$; utility buffer $\mathcal{U} \leftarrow \emptyset$; block length ℓ ; number of chirps K^i , parameters $\{\eta_\tau, \gamma_\tau\}_{\tau=1}^{\mathcal{T}}$

- 1: **for** $\tau = 1 : \mathcal{T}$ **do**
- 2: Transmission scheduling: $(f_k^i, t_k^i)_{k \in \tau} \leftarrow \text{Stochastic Round-Robin}(p_\tau^i, \ell, K^i)$ \triangleright (Subroutine 2)
- 3: Sweep subband $[f_k^i, f_k^i + B]$ over $[t_k^i, t_k^i + T_a^i]$ for each chirp $k \in \tau$
- 4: Local feedback: estimate $\overline{\text{SINR}}_\tau^i(f, t)$ (and $\overline{\text{SNR}}_\tau^i(f, t)$ when available) for all (f, t) used
- 5: Form CPI utility \bar{U}_τ^i from RX pipeline (cf. (1)), $\mathcal{U} = \mathcal{U} \cup \{\bar{U}_\tau^i\}$
- 6: Strategy update: $(p_{\tau+1}^i, \Theta_{\tau+1}^i) \leftarrow \text{Regret-Minimization}(\mathcal{U}, p_\tau^i, \Theta_\tau^i, \eta_\tau, \gamma_\tau)$ \triangleright (Subroutine 3 or 4)
- 7: **end for**

In this subsection, we develop the decentralized learning procedure from the perspective of an individual radar. Each radar observes only its own noisy measurement outcomes and lacks access to the global joint utility. Consequently, the learning process follows a form of *semi-bandit feedback*, where the local utility of a strategy is inferred from locally observable signal statistics obtained at the end of every CPI. It is termed semi-bandit because the observation from a played strategy can indirectly reveal information about the utilities of other, unplayed strategies.

We propose Algorithm 1 as the CPI-level driver that each radar executes online, which unfolds into three main procedures.

Transmission Scheduling At the beginning of CPI τ , radar i holds a mixed strategy $p_\tau^i \in \Delta(\Sigma^i)$ over strategy space. Subroutine 2 (*Stochastic Round-Robin*) then instantiates the concrete per-chirp sequence $\{(f_k^i, t_k^i)\}_{k \in \tau}$ by sampling a starting pair once per *block of chirps* and then cycling through indices within that block. This meta routine preserves temporal diversity within a CPI, and gives freedom for the design of transmission subroutine which seeks to diversify chirps but also avoid collisions.

Subroutine 2 Stochastic Round-Robin

Require: from p_τ^i get sampler $q_\tau^i(\cdot)$ over $(f, t) \in \mathcal{A}$ for CPI τ at radar i ; block length ℓ ; number of chirps K^i

- 1: **for** $b = 1$ to $\lceil K^i / \ell \rceil$ **do**
- 2: Sample starting pair $(f_s, t_s) \sim q_\tau^i(\cdot)$
- 3: **for** $l = 0$ to $\ell - 1$ **do**
- 4: $k \leftarrow (b - 1)\ell + l + 1$
- 5: $f_k^i \leftarrow f_{(s+l) \bmod A_1}, \quad t_k^i \leftarrow t_{(s+l) \bmod A_2}$
- 6: **end for**
- 7: **end for**
- 8: **return** $(f_k^i, t_k^i)_{k=1}^{K^i}$

Local Feedback and Signal Processing At the end of each CPI, the receiver computes statistics $\overline{\text{SINR}}_\tau^i(f, t)$ (and $\overline{\text{SNR}}_\tau^i$ when no interference is detected), and aggregates them into a bounded CPI utility $\bar{U}_\tau^i \in [0, 1]$, appended to the history \mathcal{U} . Specifically, we assume that at the end of CPI τ , radar i computes its signal statistics from the down-sampled and low-pass filtered ADC matrix \mathbf{Y}_τ^i , whose columns $\mathbf{Y}_{\tau,k}^i$ correspond to the received baseband signal of chirp k . This correspondence allows the radar to associate each chirp with its transmitted time-frequency configuration (f_k^i, t_k^i) and thus estimate, for every pair (f, t) , the empirical SINR as

$$\overline{\text{SINR}}_\tau^i(f, t) = \frac{\sum_k \frac{P(\tilde{\mathbf{Y}}_{\tau,k}^i) \mathbb{1}\{f_k^i = f, t_k^i = t\}}{P(\sum_{o \in \mathbf{N}(i)} \tilde{\mathbf{Y}}_{\tau,k}^o) + P(\mathbf{E}_{\tau,k}^i)}}{\sum_k \mathbb{1}\{f_k^i = f, t_k^i = t\}}, \quad (18)$$

where $\mathbf{E}_{\tau,k}^i$ denotes the receiver noise component and $\tilde{\mathbf{Y}}_{\tau,k}^o$ represents the interference signals identified from neighboring radars $o \in \mathbf{N}(i)$. We further assume that (i) the average noise power can be estimated as $N_0 = k\text{TF}$, where k is the Boltzmann constant, TF is the temperature, and F is the environment temperature; and (ii) interference components are detectable and separable by standard interference-identification techniques, enabling the estimation of $P(\sum_{o \in \mathbf{N}(i)} \tilde{\mathbf{Y}}_{\tau,k}^o)$.

When interference-free chirps are detected, the corresponding signal-to-noise ratio (SNR) can be estimated as

$$\overline{\text{SNR}}_\tau^i(f, t) = \frac{\sum_k \frac{P(\mathbf{Y}_{\tau,k}^i) \mathbb{1}\{f_k^i = f, t_k^i = t, \tilde{\mathbf{Y}}_{\tau,k}^i = \mathbf{Y}_{\tau,k}^i\}}{P(\mathbf{E}_{\tau,k}^i)}}{\sum_k \mathbb{1}\{f_k^i = f, t_k^i = t, \tilde{\mathbf{Y}}_{\tau,k}^i = \mathbf{Y}_{\tau,k}^i\}}. \quad (19)$$

These empirical SINR and SNR estimates constitute the observable performance feedback for radar i and serve as the input for its utility estimation and subsequent mixed-strategy updates.

Mixed-strategy update and regret minimization Subroutine 3 implements entropic Online Mirror Descent (OMD) [30, 36, 37] with a *bandit* (one-point) utility estimator on the strategy space Σ^i . Since each CPI samples exactly one pure strategy $\sigma_\tau^i \sim p_\tau^i$, we form the importance-weighted estimate $\hat{U}_\tau^i(\sigma) = \bar{U}_\tau^i / p_\tau^i(\sigma_\tau^i)$ if $\sigma = \sigma_\tau^i$ and 0 otherwise, which is unbiased for the linearized objective on $\Delta(\Sigma^i)$. The dual states Θ^i are updated with stepsize η_τ and projected back to the simplex by a softmax; a small exploration mass γ_τ keeps all actions played with nonzero probability (controlling estimator variance and ensuring well-posedness).

Subroutine 4 upgrades the guarantee from CCE to CE by minimizing *swap* regret on $\Delta(\Sigma^i)$. It maintains, for every source pure strategy $\sigma \in \Sigma^i$, a row-mixed-strategy $q_\sigma^i(\cdot) \in \Delta(\Sigma^i)$ that encodes how probability mass on σ would be *relabelled* to any alternative σ' . A single CPI reward \bar{U}_τ^i yields the same importance-weighted estimator $\hat{U}_\tau^i(\cdot)$ as above; then each row is updated by row-wise entropic OMD with a $p_\tau^i(\sigma)$ weighting, which is the canonical construction for no-swap-regret. Collecting the rows forms a stochastic matrix $Q_{\tau+1}^i$; the next mixed strategy $p_{\tau+1}^i$ is its left stationary distribution, i.e., the solution to $p_{\tau+1}^i = p_{\tau+1}^i Q_{\tau+1}^i$, $\sum_\sigma p_{\tau+1}^i(\sigma) = 1$.

In summary, Algorithm 1 proceeds once per CPI by (i) *generating* a time-frequency sequence via Subroutine 2 and then (ii) performing a *single* regret-based mixed-strategy update via Subroutine 3 (CCE), Subroutine 4 (CE),

Subroutine 3 Regret-Minimization (External)

Require: current strategy $p_\tau^i \in \Delta(\Sigma^i)$; CPI utility history \mathcal{U} ; stepsize $\eta_\tau > 0$; exploration $\gamma_\tau \in (0, 1)$; *dual state* Θ_τ^i storing scores $z_\tau^i(\sigma)$ for all $\sigma \in \Sigma^i$

1: Estimation: for every $\sigma \in \Sigma^i$

$$\widehat{U}_\tau^i(\sigma) \leftarrow \begin{cases} \frac{\bar{U}_\tau^i}{p_\tau^i(\sigma)} \mathbb{1}\{\sigma = \sigma_\tau^i\}, & \gamma_\tau \neq 0 \\ 1 - \frac{1 - \bar{U}_\tau^i}{p_\tau^i(\sigma)} \mathbb{1}\{\sigma = \sigma_\tau^i\}, & \gamma_\tau = 0. \end{cases}$$

2: Update:

$$z_{\tau+1}^i(\sigma) \leftarrow z_\tau^i(\sigma) + \eta_\tau \widehat{U}_\tau^i(\sigma) \quad \forall \sigma \in \Sigma^i.$$

Exploitation + exploration:

$$\begin{aligned} \tilde{p}_{\tau+1}^i(\sigma) &= \frac{\exp\{z_{\tau+1}^i(\sigma)\}}{\sum_{\sigma'} \exp\{z_{\tau+1}^i(\sigma')\}}, \\ p_{\tau+1}^i(\sigma) &= (1 - \gamma_\tau) \tilde{p}_{\tau+1}^i(\sigma) + \frac{\gamma_\tau}{|\Sigma^i|}. \end{aligned}$$

3: **Return** $p_{\tau+1}^i$ and $\Theta_{\tau+1}^i \equiv \{z_{\tau+1}^i(\sigma)\}_{\sigma \in \Sigma^i}$

Subroutine 4 Regret-Minimization (Internal)

Require: current strategy $p_\tau^i \in \Delta(\Sigma^i)$; CPI utility history \mathcal{U} ; stepsize η_τ ; exploration γ_τ ; *dual state* Ψ_τ^i storing row scores $z_{\tau,\sigma}^i(\cdot)$ and row-strategies $q_{\tau,\sigma}^i(\cdot)$ for each $\sigma \in \Sigma^i$.

1: Estimation: for every $\sigma \in \Sigma^i$

$$\widehat{U}_\tau^i(\sigma) \leftarrow \begin{cases} \frac{\bar{U}_\tau^i}{p_\tau^i(\sigma)} \mathbb{1}\{\sigma = \sigma_\tau^i\}, & \gamma_\tau \neq 0 \\ 1 - \frac{1 - \bar{U}_\tau^i}{p_\tau^i(\sigma)} \mathbb{1}\{\sigma = \sigma_\tau^i\}, & \gamma_\tau = 0. \end{cases}$$

2: Row-wise update: For each source $\sigma \in \Sigma^i$ and destination $\sigma' \in \Sigma^i$,

$$z_{\tau+1,\sigma}^i(\sigma') \leftarrow z_{\tau,\sigma}^i(\sigma') + \eta_\tau p_\tau^i(\sigma) \widehat{U}_\tau^i(\sigma').$$

3: Exploration + Exploitation:

$$\begin{aligned} \tilde{q}_{\tau+1,\sigma}^i(\sigma') &= \frac{\exp\{z_{\tau+1,\sigma}^i(\sigma')\}}{\sum_{\rho \in \Sigma^i} \exp\{z_{\tau+1,\sigma}^i(\rho)\}}, \\ q_{\tau+1,\sigma}^i(\sigma') &= (1 - \gamma_\tau) \tilde{q}_{\tau+1,\sigma}^i(\sigma') + \frac{\gamma_\tau}{|\Sigma^i|}. \end{aligned}$$

4: Assemble transition matrix: $Q_{\tau+1}^i[\sigma, \cdot] = q_{\tau+1,\sigma}^i(\cdot)$,

$$p_{\tau+1}^i = p_{\tau+1}^i Q_{\tau+1}^i, \quad \sum_{\sigma \in \Sigma^i} p_{\tau+1}^i(\sigma) = 1.$$

5: **Return** $p_{\tau+1}^i$ and $\Theta_{\tau+1}^i \equiv \{z_{\tau+1,\sigma}^i, q_{\tau+1,\sigma}^i\}_{\sigma \in \Sigma^i}$.

or any other plug-in no-regret routine. All learning occurs on the mixed-strategy simplex $\Delta(\Sigma^i)$, keeping computation light and enabling clean equilibrium statements. The stochastic round-robin sampler bridges the low-dimensional mixed-strategy (sampling starting frequency-time pairs) to physically realizable chirp schedules; hence our convergence guarantees apply to the finite game restricted to the mixed sequence strategies implementable by this sampler, faithfully reflecting the transmitter (TX)/RX architecture and the per-CPI feedback available at each radar.

3.5 Regret Analysis and Convergence Guarantee

3.5.1 External/internal-regret bound

We establish the sublinear external-regret bound in the number of CPI rounds \mathcal{T} for Subroutine 3, instantiated for any radar player $i \in \mathcal{I}$. In addition to the classical $\mathcal{O}(|\Sigma^i|^{1/2}\mathcal{T}^{1/2})$ bound that is widely seen in OMD style methods, our result demonstrates that casting an explicit constant exploration parameter will result in a larger dependence on time ($\mathcal{O}(\mathcal{T}^{2/3})$) but a milder dependence on the size of the strategy space ($\mathcal{O}(|\Sigma^i|^{1/3})$). This tradeoff is particularly well-suited to our setting where the strategy space is large but the CPI horizon \mathcal{T} is relatively limited. The bound immediately yields vanishing average regret $\mathcal{O}(\max_{i \in \mathcal{I}}\{(|\Sigma^i| \log |\Sigma^i|)^{1/3}\mathcal{T}^{2/3}\})$ and the convergence of the empirical play to the CCE set (by Corollary 1).

Theorem 1. *Fix a radar $i \in \mathcal{I}$ running Algorithm 1 with time-invariant parameters $\eta_\tau \equiv \eta$ and $\gamma_\tau \equiv \min\{\gamma_{\max}, \gamma\}$, the expected cumulative external regret for Subroutine 3 against the best fixed strategy $\sigma^* \in \Sigma^i$ obeys*

$$\mathbb{E}[\mathcal{R}_{\text{ext}}^i(\mathcal{T})] \leq \frac{\log |\Sigma^i|}{\eta} + \frac{\eta \mathcal{T} |\Sigma^i|}{\min\{\gamma_{\max}, \gamma\}} + \min\{\gamma_{\max}, \gamma\} \mathcal{T}, \quad (20)$$

where the constant $\gamma_{\max} \in (0, 1)$; for $\gamma = 0$,

$$\mathbb{E}[\mathcal{R}_{\text{ext}}^i(\mathcal{T})] \leq \frac{\log |\Sigma^i|}{\eta} + \eta \mathcal{T} |\Sigma^i|, \quad (21)$$

In particular, $\gamma := \frac{(|\Sigma^i| \log |\Sigma^i|)^{1/3}}{\mathcal{T}^{1/3}}$, $\eta := \frac{(\log |\Sigma^i|)^{2/3}}{|\Sigma^i|^{1/3} \mathcal{T}^{2/3}}$ yields

$$\mathbb{E}[\mathcal{R}_{\text{ext}}^i(\mathcal{T})] = \mathcal{O}\left(|\Sigma^i|^{1/3} \mathcal{T}^{2/3} (\log |\Sigma^i|)^{1/3}\right);$$

choosing $\gamma := 0$, $\eta := \sqrt{\frac{\log |\Sigma^i|}{|\Sigma^i| \mathcal{T}}}$ yields

$$\mathbb{E}[\mathcal{R}_{\text{ext}}^i(\mathcal{T})] = \mathcal{O}\left(|\Sigma^i|^{1/2} \mathcal{T}^{1/2} (\log |\Sigma^i|)^{1/2}\right).$$

We also prove that running Algorithm 1 with Subroutine 4 achieves sublinear internal regret, and thus yield convergence of empirical play to the CE set. The argument follows the standard reduction of swap-regret to a collection of external-regret problems on rows of strategy candidates [38], combined with a potential-function analysis for entropic OMD under importance-weighted bandit estimates.

Theorem 2. *Fix a radar $i \in \mathcal{I}$ running Algorithm 1 with time-invariant parameters $\eta_\tau \equiv \eta$ and $\gamma_\tau \equiv \min\{\gamma_{\max}, \gamma\}$, the expected cumulative internal regret for Subroutine 4 satisfies*

$$\mathbb{E}[\mathcal{R}_{\text{int}}^i(\mathcal{T})] \leq |\Sigma^i| \left(\frac{\log |\Sigma^i|}{\eta} + \frac{\eta \mathcal{T} |\Sigma^i|}{\gamma} + \gamma \mathcal{T} \right),$$

where the constant $\gamma_{\max} \in (0, 1)$; for $\gamma = 0$,

$$\mathbb{E}[\mathcal{R}_{\text{int}}^i(\mathcal{T})] \leq |\Sigma^i| \left(\frac{\log |\Sigma^i|}{\eta} + \eta \mathcal{T} |\Sigma^i| \right),$$

The two choices of η and γ in Theorem 1 yields

$$\begin{aligned} \mathbb{E}[\mathcal{R}_{\text{int}}^i(\mathcal{T})] &= \mathcal{O}\left(|\Sigma^i|^{4/3} \mathcal{T}^{2/3} (\log |\Sigma^i|)^{1/3}\right), \text{ and} \\ \mathbb{E}[\mathcal{R}_{\text{int}}^i(\mathcal{T})] &= \mathcal{O}\left(|\Sigma^i|^{3/2} \mathcal{T}^{1/2} (\log |\Sigma^i|)^{1/2}\right), \text{ respectively.} \end{aligned}$$

We defer the proofs for Theorem 1 and 2 to the Appendix.

3.5.2 Implication for Convergence

The regret bounds hence can be translated into finite-time equilibrium guarantees for the repeated game Γ restricted to the finite strategy sets $\{\Sigma^i\}_{i \in \mathcal{I}}$ (i.e., the CPI-long schedules implementable by the stochastic round-robin sampler).

Corollary 2. Let $\bar{\pi}_{\mathcal{T}}$ be the empirical joint-play distribution up to CPI \mathcal{T} over the restricted finite game with strategy sets $\{\Sigma^i\}_{i \in \mathcal{I}}$, and let

$$\varepsilon_{\text{ext}}^{(i)}(\mathcal{T}) = \frac{1}{\mathcal{T}} \mathbb{E}[\mathcal{R}_{\text{ext}}^i(\mathcal{T})], \quad \varepsilon_{\text{int}}^{(i)}(\mathcal{T}) = \frac{1}{\mathcal{T}} \mathbb{E}[\mathcal{R}_{\text{int}}^i(\mathcal{T})],$$

with $\varepsilon_{\text{ext}}(\mathcal{T}) := \max_i \varepsilon_{\text{ext}}^{(i)}(\mathcal{T})$ and $\varepsilon_{\text{int}}(\mathcal{T}) := \max_i \varepsilon_{\text{int}}^{(i)}(\mathcal{T})$. Then, if each radar runs Subroutine 3 and satisfies Theorem 1 with proper choices of $\gamma \in (0, \gamma_{\max})$ and η , then for every player i and every deviation $\hat{\sigma}^i \in \Sigma^i$, $\bar{\pi}_{\mathcal{T}}$ is an $\varepsilon_{\text{ext}}(\mathcal{T})$ -CCE, where $\varepsilon_{\text{ext}}(\mathcal{T}) = \mathcal{O}\left(\max_{i \in \mathcal{I}} |\Sigma^i|^{1/3} (\log |\Sigma^i|)^{1/3} \mathcal{T}^{-1/3}\right)$. (ii) If each radar runs Subroutine 4 and satisfies Theorem 2 with proper choices of $\gamma \in (0, \gamma_{\max})$ and η , then for every player i and every pair $\sigma^i, \sigma^{i\prime} \in \Sigma^i$, $\bar{\pi}_{\mathcal{T}}$ is an $\varepsilon_{\text{int}}(\mathcal{T})$ -CE. $\varepsilon_{\text{int}}(\mathcal{T}) = \mathcal{O}\left(\max_{i \in \mathcal{I}} |\Sigma^i|^{4/3} (\log |\Sigma^i|)^{1/3} \mathcal{T}^{-1/3}\right)$.

Proof sketch. Average the respective regret inequalities over $\tau = 1:\mathcal{T}$ for each player, divide by \mathcal{T} , and rewrite the averages as expectations under $\bar{\pi}_{\mathcal{T}}$. Part (a) is the standard external-regret \Rightarrow CCE implication (cf. Corollary 1); part (b) follows from the swap-regret \Rightarrow CE implication (cf. Lemma 1), using pairwise swap maps and conditioning on the recommended action. \square

4 Numerical Experiments

In this section, we validate the proposed No-Regret Hopping framework through comprehensive numerical simulations. We consider a challenging interference scenario and compare our approach against several baseline methods.

4.1 Experimental Setup

4.1.1 Scenario Configuration

We consider a scenario where four FMCW radars operate in close proximity. The radars are positioned randomly within a circular region of radius 25 meters around a common target located at the origin, as illustrated in Fig. 4. We assume the interference graph \mathcal{G} is fully connected, meaning each radar potentially interferes with all others. Furthermore, we assume perfect synchronization at initialization, i.e., $\Delta_{io} = 0$ for all $(i \rightarrow o) \in \mathcal{E}$, representing a worst-case scenario encountered in dense traffic conditions. This synchronized worst-case initialization tests the algorithms' ability to learn effective interference avoidance strategies from scratch.

The radar parameters are configured as follows: Each radar operates at a 77 GHz starting carrier frequency f_c . The available spectrum is divided into $A_f = 3$ frequency subbands, each with nominal bandwidth $B = 150$ MHz. The idle interval $[T_{\text{PRI}}^i - T_a^i - T_{\text{reset}}^i]$ for each radar is discretized into A_t time slots, where the time-shifting action set is defined as $\mathcal{T}_h = \{0, 2T_{\text{sett}}, 4T_{\text{sett}}, \dots, T_{\text{rst}}\}$ with $T_{\text{sett}} = 1.5 \mu\text{s}$ serving as a guard interval. This yields approximately $A_t = 7$ discrete time-shifting slots per chirp. Each radar transmits $K = 256$ chirps per CPI with pulse repetition interval $T_{\text{PRI}} = 29.99 \mu\text{s}$ and active chirp duration $T_a = 8.89 \mu\text{s}$. The radars are uniformly distributed within 5 m circles around the vertices of the polygon with radius 25 m, detecting with relative velocity v uniformly distributed within the interval of $[-25, 25] \text{ m/s}$. The target is placed uniformly randomly within the circle around the origin. The radar cross-section of the target is $\sigma_{\text{RCS}} = 20 \text{ dBsm}$. Individual radar bandwidths vary slightly within $[110, 150] \text{ MHz}$ to emulate realistic heterogeneity in automotive radar systems. Table 1 summarizes the key radar parameters used in the simulations. All simulations use a common random seed for reproducibility.

4.1.2 Algorithm Evaluation Setup

We evaluate four variants of Algorithm 1: Random Hopping (Random), Nash Equilibrium (Nash), External Regret Minimization (External), and Internal Regret Minimization (Internal). In the Random and Nash variants, the strategy-update mechanism is disabled, whereas the External and Internal variants employ Subroutines 3 and 4, respectively, for online strategy updates. To ensure a direct correspondence between mixed strategies and joint time-frequency actions, we construct each radar's strategy set Σ^i to have the same cardinality as the joint action space $\mathcal{A}_f \times \mathcal{A}_t$, with each strategy uniquely associated with a specific (f, t) pair. Under this design, sampling from $q_{\tau}^i(\cdot)$ is equivalent to sampling from $p_{\tau}^i(\cdot)$, enabling a unified treatment of pure strategies across all algorithmic variants.

1. **Random:** Each radar adopts $p_{\tau}^i = \text{Unif}(\Sigma^i)$, uniformly sample starting f - t pairs for Subroutine 2.

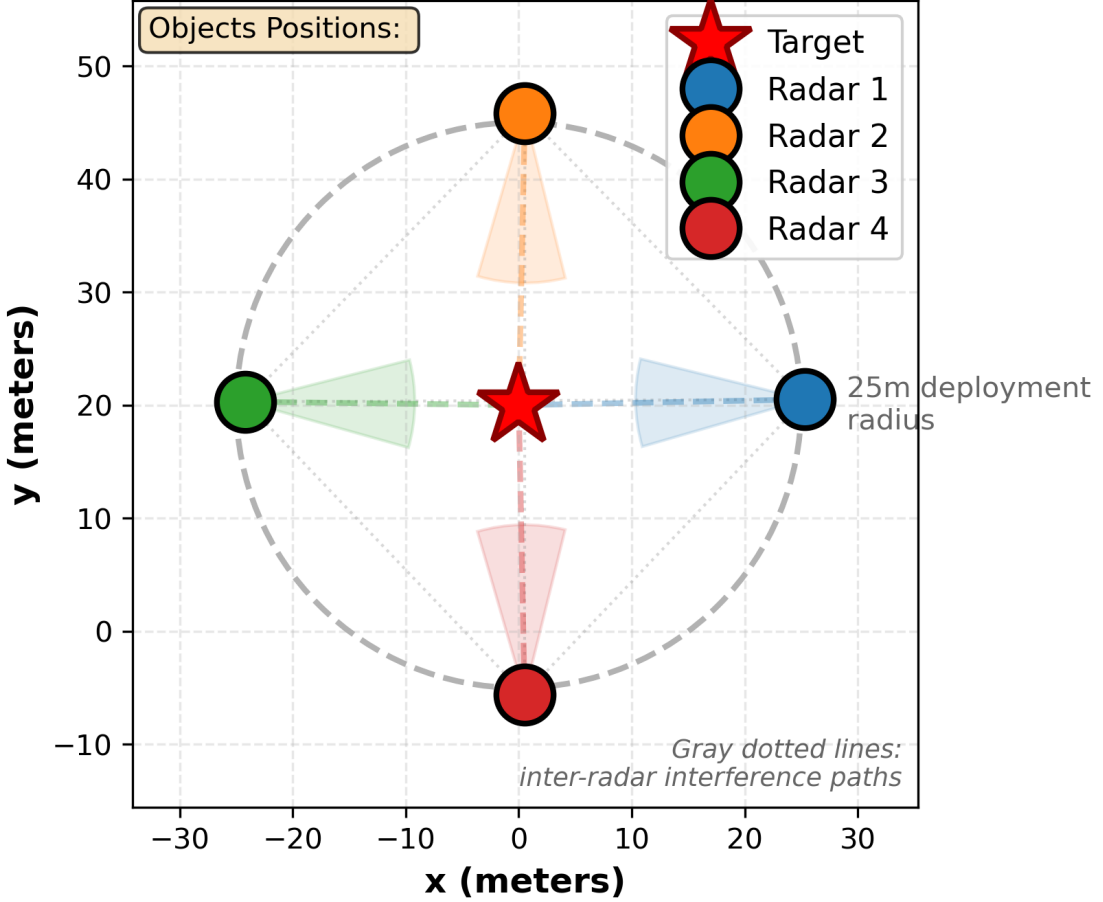


Figure 4: Example scenario: $I = 4$ radars with fully connected interference graph and synchronized operations.

Table 1: Radar System Parameters

| Parameter | Value |
|---|------------------------------|
| Frequency subbands $A_f \times$ Time slots A_t | 3×7 |
| Carrier frequency f_c (GHz) | 77 |
| Subband bandwidth B (MHz) | uniform[110, 150] |
| Active duration T_a (μ s) | 8.89 |
| Pulse repetition interval T_{PRI} (μ s) | 29.99 |
| Chirps per CPI K | 256 |
| Target range r (m) | $25 + \text{uniform}[-5, 5]$ |
| Target velocity v (m/s) | uniform[-25, 25] |
| TX power P_t (dBm) | 13 |
| Max unambiguous range R_u (m) | 200 |
| Noise power P_N (dBm) | -88 |

2. **Nash:** Each radar is assigned a unique starting frequency-time action pair deterministically throughout the blocks of Subroutine 2. We assign radar i with joint action $\text{mod}(i - 1, A_f \times A_t) + 1$. This represents perfect coordination but requires centralized coordination.
3. **External:** We use a temperature-tampered constant learning rate $\eta_\tau = \kappa \frac{\log(21)^{2/3}}{21^{1/3} \times 15^{2/3}} = 0.1252$ with the scaling constant $\kappa = 36$. Exploration rate γ_τ is set to be linearly decayed from 0.1 to 0.

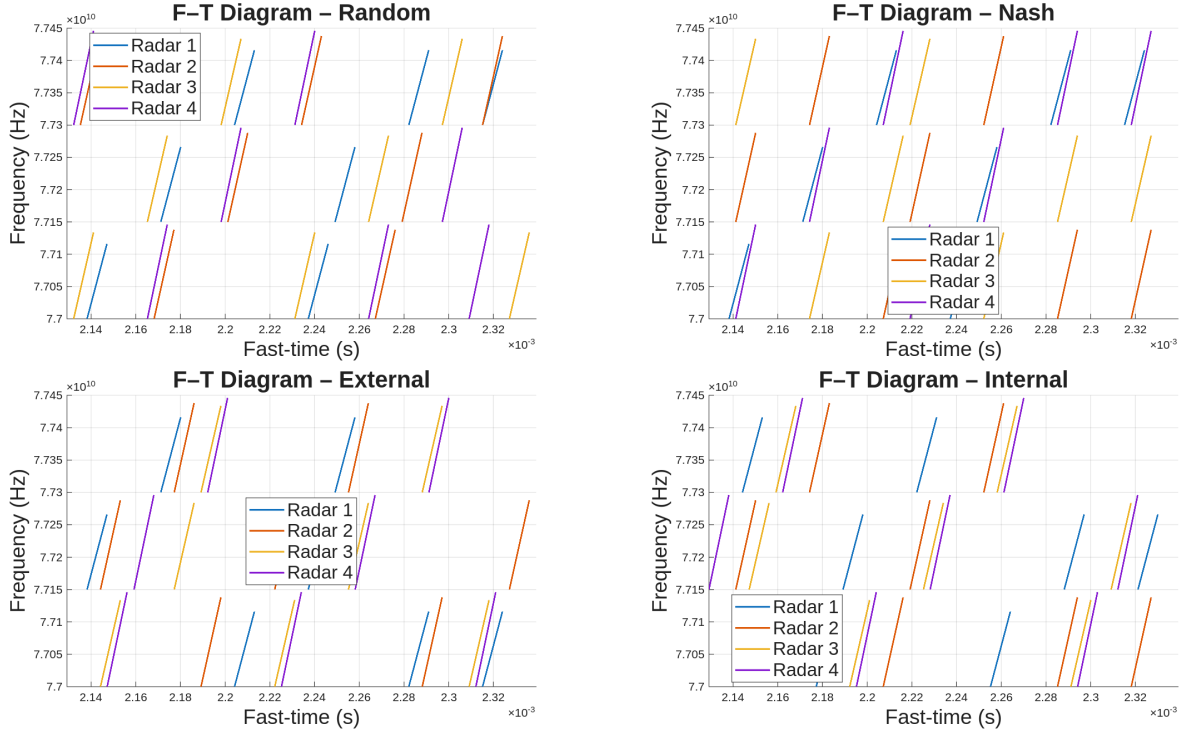


Figure 5: Frequency-time chirp illustration for different scheduling methods in the final CPI.

4. **Internal:** We set the exploration rate $\gamma_\tau \equiv 0$, and the constant learning rate for updating regret matrices to be $\eta_\tau = 0.5$. We apply a positive-part thresholding operator $[\cdot]_+$ to the score matrix z_τ^i prior to the softmax mapping at each CPI τ , in direct analogy with the Hart-Mas-Colell regret-matching construction [34].

We run 15 epochs (CPIs) for each aforementioned method, and record the last epoch performance. For learning methods, we also record the convergence behavior. The following metrics are used for the evaluation:

- SINR performance: Measured in dB, averaging the chirps of the last CPI, then averaging across the radars.
- Collision Rate: The fraction of frequency-time slots where two or more radars transmit simultaneously, normalized by the total number of slots.
- Convergence Behavior: Evolution of mixed strategies over epochs for the learning methods, visualized through strategy probability distributions. We show only the top 8 probability masses over the f - t pairs for clarity.
- Range-Doppler (RD) Map Quality: Visual assessment of target detection clarity in the 3D RD map output, with targets marked at their ground-truth positions.

4.2 Evaluation Results and Discussion

4.2.1 Frequency-Time Hopping Illustration

Fig. 5 illustrates the hopping pattern for different methods through a frequency-time diagram snapshot between intermediate chirps. In the full experiment, The random baseline exhibits uniform but highly colliding patterns, with approximately 35% of time-frequency slots experiencing collisions. The Nash joint method achieves perfect separation with zero collisions through predetermined assignments, as each radar occupies a unique frequency-time cell. Our proposed methods demonstrate intermediate behavior. The external regret minimization method learns to avoid high-collision regions, achieving approximately 3% collision rate after convergence. The internal regret minimization approach exhibits even better coordination, reaching 0% collision rate. This is due to that we set the method to be exploration-free, the seeking of a stationary distribution already gives a portion of exploration.

4.2.2 Strategy Convergence

Fig. 6 presents the evolution of mixed strategies for individual radars under the learning-based methods. Each radar's strategy is represented as a probability distribution over the $A_f \times A_t = 21$ joint actions.

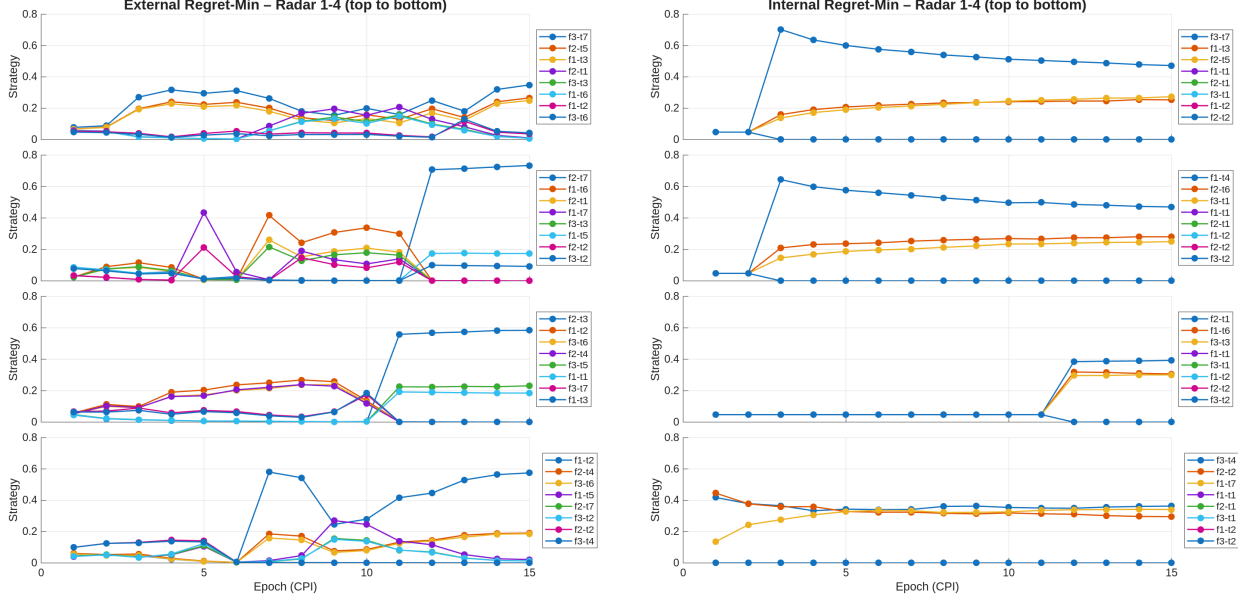


Figure 6: Evolution of mixed strategies under external (left) and internal (right) regret minimization. Only top 8 element shown.

The external regret method learns rapidly within the first 5 epochs, concentrating its strategies on a subset of high-SINR actions. By epoch 10, each radar identifies 3–5 preferred actions and focuses its probability mass accordingly. In contrast, the internal regret method's convergence is “jumper”, which is an effect attributable to the $[\cdot]_+$ operations on its regret matrices and the root-finding process for the stationary distribution. Despite this, the internal regret method ultimately achieves slightly better coordination. The final strategies for both methods exhibit implicit correlation, as radars learn to select complementary actions that minimize mutual interference.

4.2.3 Final CPI Results

Figure 7 presents the final converged RD maps for a representative radar under the different scheduling methods. The results clearly illustrate the distinctive behaviors of each approach. The random method fails to avoid interference, leading to a significant elevation of the noise floor across the RD map and causing the target response to be entirely submerged. The Nash method, although theoretically free of collisions, exhibits noticeable Doppler aliasing. This artifact arises from the deterministic periodic frequency assignment produced by its round-robin strategy (Algorithm 2). In contrast, the regret-based methods deliver substantially improved performance. Both external and internal regret minimization successfully learn interference-avoiding patterns.

Regarding collision statistics, the Nash method attains a collision rate of zero, consistent with its design. The two regret-based methods progressively reduce their collision rates over training, with the internal regret method driving the rate to zero within approximately 12 epochs. The random method, by comparison, maintains a persistently high collision rate due to its independent uniform sampling of time–frequency actions.

4.2.4 SINR Performance

We extended the radar configuration to scenarios of 3–7 radars, and performed 50 Monte-Carlo (MC) trials for each algorithm in each scenario, recording the average SINR across radars and the standard deviation across trials. The results are plotted in Fig. 8.

We observe that the random baseline produces the lowest SINR (approx. 28, 25, 22, 19, and 16 dB for 3–7 radars), a result inherent to its time-shifting design. Although the Nash single-band method has the highest theoretical SINR, it is empirically outperformed by both external and internal regret minimization methods. Between the two regret minimization approaches, no explicit performance advantage was evident.

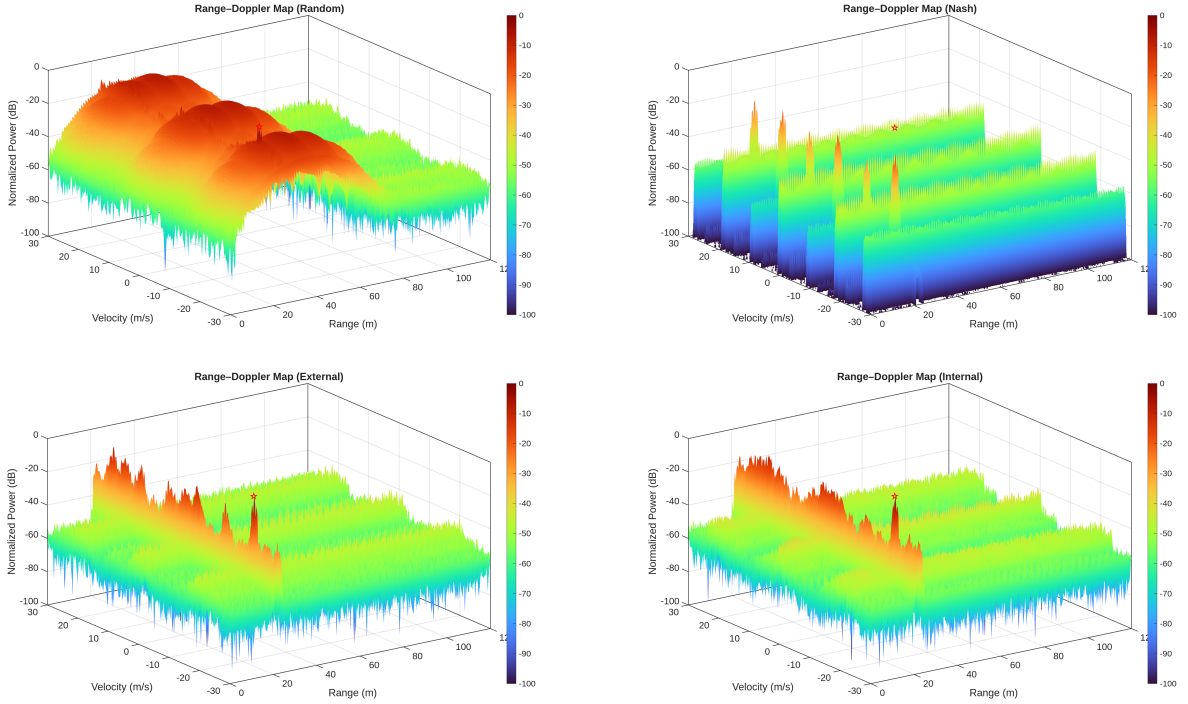


Figure 7: The final CPI RD maps for an individual radar operating with different methods.

Overall, both regret-based methods reliably learn collision-free time–frequency patterns and deliver higher SINR and clearer RD maps than the randomized and Nash baselines, demonstrating the effectiveness of joint time–frequency no-regret scheduling in dense multi-radar environments.

5 Conclusion

We have introduced a game-theoretic framework for proactive interference avoidance in automotive FMCW radar networks, generalizing previous frequency-hopping schemes to include time-domain shifts. By modeling joint time–frequency scheduling as a repeated anti-coordination game, we developed a decentralized no-regret learning algorithm that enables each radar to autonomously adapt chirp start times and subband selections without communication. We proved sublinear external and internal regret bounds and established convergence of the empirical play to coarse correlated or correlated equilibria. Numerical experiments demonstrated that leveraging both temporal and spectral degrees of freedom significantly reduces collision rates and improves SINR and range–Doppler fidelity compared to randomized time–frequency dithering and centralized Nash-based strategies. These results highlight the practicality and scalability of no-regret time–frequency scheduling for dense automotive radar scenarios. Future work will explore heterogeneous radar capabilities, more realistic channel models, and hardware-in-the-loop validation on production platforms.

Acknowledgment

The authors used generative AI models gemini-2.5-pro and ChatGPT-5 for minor language editing. All technical content, analysis, and conclusions were developed by the authors.

Proof of Theorem 1. Let $w_\tau(\sigma) := \exp\{z_\tau^i(\sigma)\}$ and $W_\tau := \sum_\sigma w_\tau(\sigma)$, so $\tilde{p}_\tau^i(\sigma) = w_\tau(\sigma)/W_\tau$. By the update rule and setting $\eta \leq \gamma/|\Sigma^i|$, we have $\eta \widehat{U}_\tau^i(\sigma) \in [0, 1]$ (since $\widehat{U}_\tau^i(\sigma) \leq 1/p_\tau^i(\sigma_\tau) \leq |\Sigma^i|/\gamma$). For any $x \in [0, 1]$,

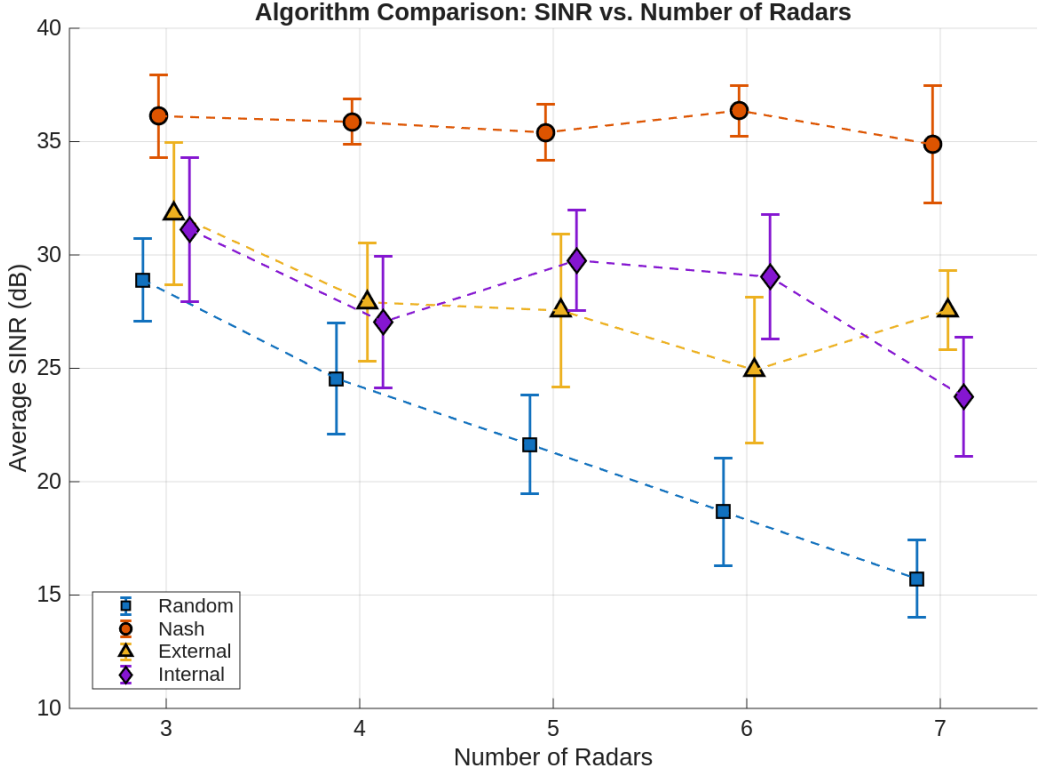


Figure 8: Average SINR comparison for all methods. The error bars represent the standard deviation of the per-trial mean SINR, computed across all radars.

$e^x \leq 1 + x + x^2$. Hence,

$$\begin{aligned}
 W_{\tau+1} &= \sum_{\sigma} w_{\tau}(\sigma) \exp\{\eta \widehat{U}_{\tau}^i(\sigma)\} \\
 &\leq \sum_{\sigma} w_{\tau}(\sigma) \left(1 + \eta \widehat{U}_{\tau}^i(\sigma) + \eta^2 \widehat{U}_{\tau}^i(\sigma)^2\right) \\
 &= W_{\tau} \left(1 + \eta \langle \tilde{p}_{\tau}^i, \widehat{U}_{\tau}^i \rangle + \eta^2 \sum_{\sigma} \tilde{p}_{\tau}^i(\sigma) \widehat{U}_{\tau}^i(\sigma)^2\right).
 \end{aligned}$$

Taking logs and using $\log(1 + x) \leq x$,

$$\log W_{\tau+1} - \log W_{\tau} \leq \eta \langle \tilde{p}_{\tau}^i, \widehat{U}_{\tau}^i \rangle + \eta^2 \sum_{\sigma} \tilde{p}_{\tau}^i(\sigma) \widehat{U}_{\tau}^i(\sigma)^2. \quad (22)$$

On the other hand, for any fixed comparator σ^* ,

$$\log \frac{w_{\tau+1}(\sigma^*)}{W_1} = \sum_{\tau=1}^{\mathcal{T}} \eta \widehat{U}_{\tau}^i(\sigma^*) - \sum_{\tau=1}^{\mathcal{T}} (\log \frac{W_{\tau+1}}{W_{\tau}}).$$

Combining with (22) and using $W_1 = |\Sigma^i|$ and $w_{\tau+1}(\sigma^*) \leq W_{\tau+1}$ gives

$$\sum_{\tau=1}^{\mathcal{T}} \langle \tilde{p}_{\tau}^i, \widehat{U}_{\tau}^i \rangle - \widehat{U}_{\tau}^i(\sigma^*) \leq \frac{\log |\Sigma^i|}{\eta} + \eta \sum_{\tau=1}^{\mathcal{T}} \sum_{\sigma} \tilde{p}_{\tau}^i(\sigma) \widehat{U}_{\tau}^i(\sigma)^2. \quad (23)$$

We now take expectations w.r.t. the learner's sampling. By standard importance-weighting, and the unbiasedness of utility estimation $\mathbb{E}_{\tau-1}[\widehat{U}_{\tau}^i(\sigma)] = \mathbb{E}_{\tau-1}[\widehat{U}_{\tau}^i(\sigma)] = U_{\tau}^i$, $\mathbb{E}_{\tau-1}[\langle \tilde{p}_{\tau}^i, \widehat{U}_{\tau}^i \rangle] = \mathbb{E}_{\tau-1}[\langle \tilde{p}_{\tau}^i, U_{\tau}^i \rangle]$. For the quadratic term,

note that only the played arm contributes. Therefore, when $\gamma \neq 0, \gamma \leq \gamma_{\max}$:

$$\sum_{\sigma} \tilde{p}_{\tau}^i(\sigma) \hat{U}_{\tau}^i(\sigma)^2 = \tilde{p}_{\tau}^i(\sigma_{\tau}) \frac{\bar{U}_{\tau}^i(\sigma_{\tau})^2}{p_{\tau}^i(\sigma_{\tau})^2} \leq \frac{1}{p_{\tau}^i(\sigma_{\tau})} \leq \frac{|\Sigma^i|}{\gamma},$$

since $U_{\tau}^i(\sigma_{\tau}) \leq 1$, and $p_{\tau}^i \geq \gamma \mathbf{1}/|\Sigma^i|$. Therefore

$$\mathbb{E} \left[\sum_{\tau=1}^{\mathcal{T}} \sum_{\sigma} \tilde{p}_{\tau}^i(\sigma) \hat{U}_{\tau}^i(\sigma)^2 \right] \leq \frac{\mathcal{T}|\Sigma^i|}{\gamma}.$$

Taking expectations in (23) and using $\langle p_{\tau}^i, U_{\tau}^i \rangle = (1 - \gamma) \langle \tilde{p}_{\tau}^i, U_{\tau}^i \rangle + \gamma \langle \mathbf{1}/|\Sigma^i|, U_{\tau}^i \rangle \geq (1 - \gamma) \langle \tilde{p}_{\tau}^i, U_{\tau}^i \rangle$ (hence $\langle \tilde{p}_{\tau}^i, U_{\tau}^i \rangle \leq \langle p_{\tau}^i, U_{\tau}^i \rangle + \gamma$), we obtain

$$\mathbb{E} \left[\sum_{\tau=1}^{\mathcal{T}} U_{\tau}^i(\sigma^*) - \langle p_{\tau}^i, U_{\tau}^i \rangle \right] \leq \frac{\log |\Sigma^i|}{\eta} + \frac{\eta \mathcal{T} |\Sigma^i|}{\gamma} + \gamma \mathcal{T}.$$

Rearranging gives (20). Optimizing the RHS over η and then γ yields the stated $\mathcal{O}(\mathcal{T}^{2/3} |\Sigma^i|^{1/3} (\log |\Sigma^i|)^{1/3})$ bound.

When $\gamma = 0$,

$$\sum_{\sigma} \tilde{p}_{\tau}^i(\sigma) \hat{U}_{\tau}^i(\sigma)^2 \leq (1 - \bar{U}_{\tau}^i)^2 + \sum_{\sigma^i \neq \sigma_{\tau}^i} \bar{U}_{\tau}^i(\sigma^i, \sigma_{\tau}^{-i}) \leq |\Sigma^i|.$$

Taking expectations in (23), we obtain

$$\mathbb{E} \left[\sum_{\tau=1}^{\mathcal{T}} U_{\tau}^i(\sigma^*) - \langle p_{\tau}^i, U_{\tau}^i \rangle \right] \leq \frac{\log |\Sigma^i|}{\eta} + \eta \mathcal{T} |\Sigma^i|,$$

Optimizing the RHS over η and then γ yields the stated $\mathcal{O}(\sqrt{\mathcal{T} |\Sigma^i| \log |\Sigma^i|})$ bound. \square

Proof of Theorem 2. We show the stated bound on the internal regret for a fixed radar i . For each source action $\sigma \in \Sigma^i$, we define the *row-wise* vector:

$$v_{\tau, \sigma}^i(\sigma') := p_{\tau}^i(\sigma)(\sigma') U_{\tau}^i(\sigma'),$$

for every pure strategy σ^i where $U_{\tau}^i(\cdot) \in [0, 1]^{|\Sigma^i|}$ is the true utility vector at CPI τ for player i , and $p_{\tau}^i \in \Delta(\Sigma^i)$ is the mixed strategy used at that CPI. Now, the algorithm has access only to bandit feedback via the estimator \hat{U}_{τ}^i of U_{τ}^i , according to which we can define estimator $\hat{v}_{\tau}^i(\sigma') := p_{\tau}^i(\sigma) \hat{U}(\sigma')$. We claim that $v_{\tau, \sigma}^i(\sigma')$ satisfies the following property: $\mathbb{E}_{\tau-1}[\hat{v}(\sigma')] = p_{\tau}^i U_{\tau}(\sigma')$

For each fixed source $\sigma \in \Sigma^i$, Subroutine 4 runs a bandit external optimizer on the row game with reward vectors $v_{\tau, \sigma}^i$, with utility estimator $\hat{v}_{\tau, \sigma}^i$. Let $q_{\tau, \sigma}^i \in \Delta(\Sigma^i)$ denote the row strategy at CPI τ for source σ , applying Theorem 1 *row-wise* yields: for any fixed $\sigma \in \Sigma^i$ and any comparator $\sigma' \in \Sigma^i$,

$$\begin{aligned} \mathbb{E} \left[\sum_{\tau=1}^{\mathcal{T}} v_{\tau, \sigma}^i(\sigma') - \langle q_{\tau, \sigma}^i, v_{\tau, \sigma}^i \rangle \right] &\leq \frac{\log |\Sigma^i|}{\eta} + \frac{\eta |\Sigma^i|}{\gamma} \mathcal{T} + \gamma \mathcal{T}, \\ \text{or when } \gamma \equiv 0 &\leq \frac{\log |\Sigma^i|}{\eta} + \eta \mathcal{T} |\Sigma^i|, \end{aligned}$$

where we have taken a constant learning rate $\eta_{\tau} \equiv \eta$ and exploration rate $\gamma_{\tau} \equiv \min\{\gamma_{\max}, \gamma\}$ for simplicity.

Invoking the external-to-swap regret reduction of Blum & Mansour [38, Theorem 5], we obtain,

$$\begin{aligned} \mathcal{R}_{\text{int}}^i(\mathcal{T}) &= \max_{\phi} \sum_{\tau=1}^{\mathcal{T}} \langle p_{\tau}^i(\cdot), U_{\tau}^i(\phi(\cdot)) - U_{\tau}^i(\cdot) \rangle \\ &= \max_{\phi} \sum_{\tau=1}^{\mathcal{T}} \langle p_{\tau}^i(\cdot), Q_{\tau}^i U_{\tau}^i(\phi(\cdot)) - Q_{\tau}^i U_{\tau}^i(\cdot) \rangle \\ &= \max_{\phi} \sum_{\sigma \in \Sigma^i} \sum_{\tau=1}^{\mathcal{T}} p_{\tau}^i(\sigma) (U_{\tau}^i(\phi(\sigma)) - \langle q_{\tau, \sigma}^i(\cdot), U_{\tau}^i(\cdot) \rangle) \\ &\leq \sum_{\sigma \in \Sigma^i} \max_{\sigma'} \sum_{\tau=1}^{\mathcal{T}} (v_{\tau, \sigma}^i(\sigma') - \langle q_{\tau, \sigma}^i(\cdot), v_{\tau, \sigma}^i(\cdot) \rangle), \end{aligned}$$

where we eliminate the \max_ϕ by exchange the order of the inner product and summation over \mathcal{T} . Now each source pure strategy σ corresponds to an external minimizer.

Therefore, by applying the row-wise result, we arrive at

$$\begin{aligned}\mathbb{E}[\mathcal{R}_{\text{int}}^i(\mathcal{T})] &\leq |\Sigma^i| \left(\frac{\log |\Sigma^i|}{\eta} + \frac{\eta |\Sigma^i|}{\gamma} \mathcal{T} + \gamma \mathcal{T} \right), \text{ or} \\ \mathbb{E}[\mathcal{R}_{\text{int}}^i(\mathcal{T})] &\leq |\Sigma^i| \left(\frac{\log |\Sigma^i|}{\eta} + \eta |\Sigma^i| \mathcal{T} \right),\end{aligned}$$

where we simply apply the fact that $p_\tau^i \leq 1$, and use the result for the external regret bound. Now the results are almost immediate, e.g., treating γ as a constant and optimizing over η , we have $\eta = \sqrt{\frac{\gamma \log |\Sigma^i|}{(|\Sigma^i| \mathcal{T})}}$. Plugging the η expression back in and optimizing γ we obtain $\gamma = \left(\sqrt{\frac{|\Sigma^i| \log |\Sigma^i|}{\mathcal{T}}} \right)^{2/3}$, hence choosing $\eta = (\log |\Sigma^i|)^{2/3} |\Sigma^i|^{-1/3} \mathcal{T}^{-2/3}$ yields the stated internal regret bound. \square

References

- [1] S. Sun, A. P. Petropulu, and H. V. Poor, “MIMO radar for advanced driver-assistance systems and autonomous driving: Advantages and challenges,” *IEEE Signal Processing Magazine*, vol. 37, no. 4, pp. 98–117, 2020.
- [2] S. Sun and Y. D. Zhang, “4D automotive radar sensing for autonomous vehicles: A sparsity-oriented approach,” *IEEE Journal of Selected Topics in Signal Processing*, vol. 15, no. 4, pp. 879–891, 2021.
- [3] S. Rao, R. Narasimha, and S. Sun, “Signal processing challenges in automotive radar,” in *IEEE International Conference on Acoustics, Speech and Signal Processing (ICASSP)*, 2025, pp. 1–5.
- [4] L. Xu, S. Sun, K. V. Mishra, and Y. D. Zhang, “Automotive FMCW radar with difference co-chirps,” *IEEE Transactions on Aerospace and Electronic Systems*, vol. 59, no. 6, pp. 8145–8165, 2023.
- [5] R. Zheng, S. Sun, H. Liu, and T. Wu, “Deep-neural-network-enabled vehicle detection using high-resolution automotive radar imaging,” *IEEE Transactions on Aerospace and Electronic Systems*, vol. 59, no. 5, pp. 4815–4830, 2023.
- [6] M. Markel, *Radar for Fully Autonomous Driving*. Boston, MA: Artech House, 2022.
- [7] J. Li, R. Wu, I.-T. Lu, and D. Ren, “Bayesian linear regression with cauchy prior and its application in sparse mimo radar,” *IEEE Transactions on Aerospace and Electronic Systems*, vol. 59, no. 6, pp. 9576–9597, 2023.
- [8] T. Li, H. Lei, and Q. Zhu, “Self-adaptive driving in nonstationary environments through conjectural online lookahead adaptation,” in *2023 IEEE International Conference on Robotics and Automation (ICRA)*, 2023, pp. 7205–7211.
- [9] G. Hakobyan and B. Yang, “High-performance automotive radar: A review of signal processing algorithms and modulation schemes,” *IEEE Signal Processing Magazine*, vol. 36, no. 5, pp. 32–44, 2019.
- [10] W. Buller, B. Wilson, J. Garbarino, J. Kelly, B. Thelen, B. M. Belzowski *et al.*, “Radar congestion study,” United States. Department of Transportation. National Highway Traffic Safety ..., Tech. Rep., 2018.
- [11] A. Ossowska, L. Sit, S. Manchala, T. Vogler, J. Vanova, J. Hejtmanek, K. Krupinski, and U. Luebbert, “Imiko-radar: Interference measurements of today’s automotive radar sensors,” in *2021 21st International Radar Symposium (IRS)*. IEEE, 2021, pp. 1–6.
- [12] J. Li, J. Youn, R. Wu, J. Overdevest, and S. Sun, “Performance evaluation and analysis of thresholding-based interference mitigation for automotive radar systems,” in *2024 IEEE International Conference on Acoustics, Speech, and Signal Processing Workshops (ICASSPW)*, 2024, pp. 204–208.
- [13] R. H. Wu, J. Li, M. Brett, and M. A. Staudenmaier, “Radar communication with interference suppression,” Nov. 3 2022, US Patent App. 17/245,613.
- [14] W. Li, H. Zhang, J. Wang, and X. Liu, “An interference mitigation method for fmcw radar based on time-frequency distribution and dual-domain fusion filtering,” *Sensors*, vol. 24, no. 11, p. 3288, 2024.
- [15] J. Youn, J. Li, R. Wu, and J. Overdevest, “Interference mitigation evaluation methodology for automotive radar,” in *2024 21st European Radar Conference (EuRAD)*, 2024, pp. 115–118.

- [16] F. Laghezza, F. Jansen, and J. Overdevest, “Enhanced interference detection method in automotive FMCW radar systems,” in *2019 20th International Radar Symposium (IRS)*, 2019, pp. 1–7.
- [17] X. Wei, J. Overdevest, J. Li, J. Youn, S. Ravindran, and R. J. Van Sloun, “Score-based generative modeling for interference mitigation in automotive fmcw radar,” in *2024 21st European Radar Conference (EuRAD)*, 2024, pp. 27–30.
- [18] X. Wei, J. Youn, J. Overdevest, J. Li, S. Ravindran, and R. J. van Sloun, “Deep unfolding using score-based generative networks for automotive radar interference mitigation,” in *ICASSP 2025 - 2025 IEEE International Conference on Acoustics, Speech and Signal Processing (ICASSP)*, 2025, pp. 1–5.
- [19] J. Mun, S. Ha, and J. Lee, “Automotive radar signal interference mitigation using RNN with Self Attention,” in *ICASSP 2020 - 2020 IEEE International Conference on Acoustics, Speech and Signal Processing (ICASSP)*, 2020, pp. 3802–3806.
- [20] W. Chen, Y. Zhang, and Q. Li, “Deep learning for interference mitigation in time-frequency maps of fmcw radars,” in *2023 IEEE International Radar Conference (RADAR)*. IEEE, 2023, pp. 1–6.
- [21] Y. D. Zhang and S. Sun, “Identical partitioning of consecutive integer set,” in *2024 IEEE 13rd Sensor Array and Multichannel Signal Processing Workshop (SAM)*, 2024, pp. 1–5.
- [22] Y. Stettiner and N. Arkind, “FMCW automotive radar incorporating nonlinear frequency hopping sequence of fractional bandwidth multiband chirps,” Mar. 21 2023, US Patent 11,609,303.
- [23] J. Khoury, R. Ramanathan, D. McCloskey, R. Smith, and T. Campbell, “RadarMAC: Mitigating radar interference in self-driving cars,” in *2016 13th Annual IEEE International Conference on Sensing, Communication, and Networking (SECON)*, 2016, pp. 1–9.
- [24] S. Jin and S. Roy, “FMCW radar network: Multiple access and interference mitigation,” *IEEE Journal of Selected Topics in Signal Processing*, vol. 15, no. 4, pp. 968–979, 2021.
- [25] Y. Pan, J. Li, L. Xu, S. Sun, and Q. Zhu, “A game-theoretic approach for high-resolution automotive FMCW radar interference avoidance,” in *2025 IEEE International Radar Conference (RADAR)*, 2025, pp. 1–6.
- [26] T. Başar and G. J. Olsder, *Dynamic Noncooperative Game Theory*. SIAM, 1998.
- [27] T. Roughgarden, *Algorithmic Game Theory*. ACM New York, NY, USA, 2010, vol. 53, no. 7.
- [28] C. Daskalakis, P. W. Goldberg, and C. H. Papadimitriou, “The complexity of computing a nash equilibrium,” *SIAM Journal on Computing*, vol. 39, no. 1, pp. 195–259, 2009. [Online]. Available: <https://doi.org/10.1137/070699652>
- [29] Y. Pan, T. Li, and Q. Zhu, “On the resilience of traffic networks under non-equilibrium learning,” in *2023 American Control Conference (ACC)*. IEEE, 2023, pp. 3484–3489.
- [30] ———, “On the variational interpretation of mirror play in monotone games,” in *2024 IEEE 63rd Conference on Decision and Control (CDC)*, 2024, pp. 6799–6804.
- [31] T. Li, G. Peng, Q. Zhu, and T. Başar, “The confluence of networks, games, and learning a game-theoretic framework for multiagent decision making over networks,” *IEEE Control Systems*, 2022.
- [32] Y. Pan and Q. Zhu, “Efficient episodic learning of nonstationary and unknown zero-sum games using expert game ensembles,” in *2021 60th IEEE Conference on Decision and Control (CDC)*, 2021, pp. 1669–1676.
- [33] L. Xu, S. Sun, K. V. Mishra, and Y. D. Zhang, “Automotive fmcw radar with difference co-chirps,” *IEEE Transactions on Aerospace and Electronic Systems*, vol. 59, no. 6, pp. 8145–8165, 2023.
- [34] S. Hart and A. Mas-Colell, “A simple adaptive procedure leading to correlated equilibrium,” *Econometrica*, vol. 68, no. 5, pp. 1127–1150, 2000.
- [35] N. Cesa-Bianchi and G. Lugosi, *Prediction, learning, and games*. Cambridge university press, 2006.
- [36] Y. Pan, T. Li, and Q. Zhu, “Is stochastic mirror descent vulnerable to adversarial delay attacks? A traffic assignment resilience study,” in *2023 62nd IEEE Conference on Decision and Control (CDC)*, 2023, pp. 8328–8333.
- [37] S. Liu, T. Li, and Q. Zhu, “Game-theoretic distributed empirical risk minimization with strategic network design,” *IEEE Transactions on Signal and Information Processing over Networks*, vol. 9, pp. 542–556, 2023.
- [38] A. Blum and Y. Mansour, “From external to internal regret,” *Journal of Machine Learning Research*, vol. 8, no. 47, pp. 1307–1324, 2007. [Online]. Available: <http://jmlr.org/papers/v8/blum07a.html>